1949

Mass-Remainder Analysis (MARA) in the characterization of polymers and epoxidized oils

Ph.D. Dissertation

Mahir Hashimov

Supervisor: Prof. Dr. Sándor Kéki

`

UNIVERSITY OF DEBRECEN

Doctoral Council of Natural Sciences and Information Technology

Doctoral School of Chemistry

Debrecen, 2022

Declaration

Hereby I, Mahir Hashimov, declare that I prepared this dissertation within the program of Debrecen University, Doctoral Council of Natural Sciences and Information Technology, Doctoral school of chemistry, Macromolecular and Surface Chemistry Program K/4 in order to obtain a PhD Degree in Natural Sciences/Informatics at Debrecen University. Herewith I declare that the results published in the dissertation are not reported in any other PhD dissertation(s).

Debrecen, 2022 signature of the candidate

Hereby I, Sándor Kéki, confirm that candidate, Mahir Hashimov has conducted his research under my supervision within the K/4 Doctoral Program of the Doctoral School of Chemistry between 2018 and 2022. The independent studies and research activity of the candidate significantly contributed to the results published in the dissertation. I also declare that the results published in the dissertation are not reported in any other dissertation(s). I recommend the approval of his dissertation.

Debrecen, 2022 signature of the supervisor

Mass-Remainder Analysis (MARA) in the characterization of polymers and epoxidized oils

Dissertation submitted in partial fulfilment of the requirements for the doctoral (PhD) degree in the field of Chemistry

Written by: **Mahir Hashimov** (certified chemist)

Prepared in the framework of the Doctoral School of Chemistry of the University of Debrecen

(K/4 Macromolecular and Surface Chemistry programme)

Dissertation advisor: **Prof. Dr. Sándor Kéki**

The official opponents of the dissertation:

Dr. …….. ……..
Dr. …….. ……..
Dr. …….. ……..

The evaluation committee:

Chairperson:	Dr. ……	……..
Members:	Dr. ……	……..
	Dr. ……	……..
	Dr. ……	……..
	Dr. ……	……..

The date of the dissertation defence: 2022

Dedicated to memory of my beloved mother

ACKNOWLEDGEMENTS

First and foremost, I want to thank my supervisor Prof. Dr. Sándor Kéki to offer me this opportunity to become his Ph.D. student and to have "Dr" status before my name. I also appreciate him for his unique contribution and strategic management as a Head of Applied Chemistry Department. It is not possible to forget Dr. Tibor Nagy's continuous encouragement, valuables advice, assistance, and unfunny jokes throughout my PhD years.

During these years I gained lots of theoretical and practical knowledge and improved my personal development skills. First time I participated in scientific conferences. This allowed me to develop my communication skills, enthusiasm, and the ability to engage with an audience and to explore different European and Hungarian cities.

I would like to acknowledge all Debrecen University professors and lecturers specially Dr. György Deák, Dr. Ákos Kuki and Dr. Lajos Nagy to teach me and share their scientific experiences.

I gratefully thank Tempus Public Foundation that honoured me with Stipendium Hungaricum scholarship to fund my tuition fee and living expenses during my studies between 2018-2022.

Last but not least I would like to thank my friends, who supported me in all pursuits with love and believed in my success. And most of all my encouraging and inspiriting brother Ülvi who is my lifelong friend.

This work was supported by GINOP-2.3.2-15-2016-00041, GINOP 2.3.3-15-2016-00021, GINOP-2.3.3-15-2016-00004, EFOP-3.6.1-16-2016-00022 projects as well as No. FK-132685 and No. FK-132385 grants by from National Research, Development and Innovation Office (NKFI) and Thematic Excellence Programme of the Ministry for Innovation and Technology of

Hungary (ED_18-1-2019-0028), within the framework of the Vehicle Industry Thematic Programme of the University of Debrecen.

Mahir Hashimov
Debrecen, Hungary

“Equipped with our five senses, along with telescopes and microscopes and mass spectrometers and seismographs and magnetometers and particle accelerators and detectors across the electromagnetic spectrum, we explore the universe around us and call the adventure science.”

Neil DeGrasse Tyson - an American astrophysicist, planetary scientist, author, and science communicator

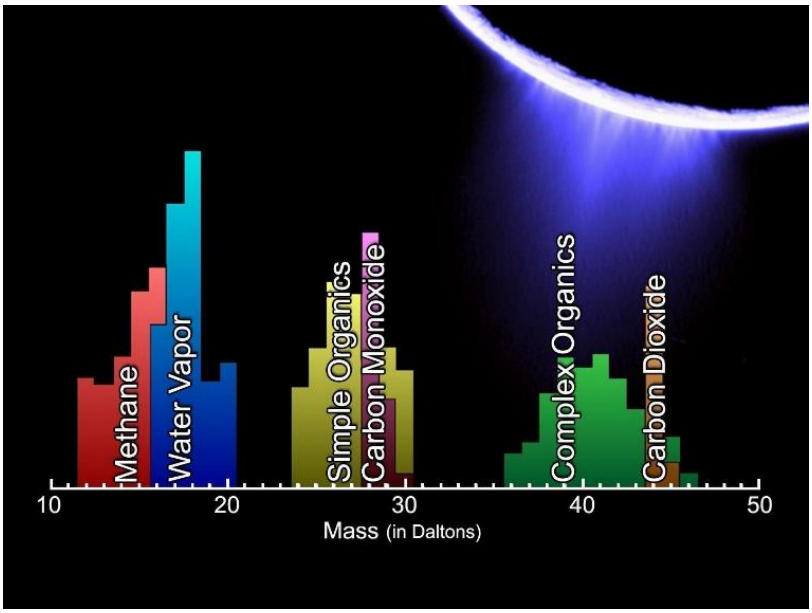

The lower panel is a mass spectrum that shows the chemical constituents sampled in Enceladus' plume by Cassini's Ion and Neutral Mass Spectrometer during its fly-through of the plume on Mar. 12, 2008.

Credit: **NASA Science - SOLAR SYSTEM EXPLORATION**

LIST OF ABBREVATIONS

CCV	Characteristic collision voltage
CID	Collision-induced dissociation
DBE	Double bond equivalent
DHB	2,5-Dihydroxybenzoic acid
DOE	Degree of epoxidation
EFA	Epoxidized fatty acid
ELA	Epoxidized linoleic acid
ELNA	Epoxidized linolenic acid
EO	Ethylene oxide
EOA	Epoxidized oleic acid
ESBO	Epoxidized soybean oil
ESI-QTOF	Electrospray ionization Quadrupole-Time-of-Flight
ETG	Epoxidized triglyceride
MALDI-TOF MS	Matrix-Assisted Laser Desorption Ionization Time-of-Flight Mass Spectrometry
MARA	Mass-Remainder Analysis
MCP	Microchannel plate
M_n	Number average molecular weight
MR	Mass remainder

MS/MS	Tandem mass spectrometry
NaTFA	Sodium trifluoroacetate
NEG	Number of epoxide groups
PEG	Polyethylene glycol
PLA/PCL	Polylactide/polycaprolactone
PO	Propylene oxide
PPG	Polypropylene glycol
ROP	Ring-opening polymerization
SA	Stearic acid
SY	Survival yield
TAMARA	Tandem Mass-Remainder Analysis
THAP	Trihydroxyacetophenone

TABLE OF CONTENTS

1. INTRODUCTION AND OBJECTIVES

Mass spectrometry is one of the best methods to analyse complex chemical mixture and compounds. As a compound becomes more complex, it is complicated to evaluate the spectrum. To solve this issue, we apply recently invented data mining method - Mass-Remainder Analysis (MARA) and develop it further to Tandem Mass-Remainder Analysis (TAMARA) to get a simplified graphical representation of the MS/MS spectra.

In our research we perform mass spectrometric measurements on different types of polymers such as polyether polyols, various polymer blending and copolymers, and epoxidized vegetable oils. **Figure 1** briefly demonstrates our work plan and describes the most important points during the research.

Nowadays, increasing of plastic waste causes a big eco problem on our planet. That's why there is a big demand on the production of biodegradable polymers. Since epoxidized vegetable oils can undergo photopolymerization reaction to produce biopolymers, the characterization of these compounds is very important to propose new materials.

We measure the epoxidized soybean and linseed oils with ESI-QTOF and MALDI-TOF mass spectrometers and characterize them by applying mass-remainder analysis. We determine the number of carbon atoms and epoxide groups, the degree of epoxidation as well as applying tandem mass spectrometry we study the fragmentation mechanisms and propose the fragmentation pathways for the sodium and ammonium ETG adducts.

As another part of our research, we investigate the copolymer blends. A wide range of demands for various applications of blending polymers makes it necessary to study and explore them. We study random or block types of different blends with average molecular weight up to 3000 Da. We develop

multi-step mass-remainder analysis method, which produces a simplified graphical representation of the complex mass spectra, to comprehend between samples consisting of a single copolymer or blend of copolymers as well as the similarities or differences in the chemical compositions. This method allows us to assign elemental composition of EO/PO copolymers easily and fast as well as to filter the different homopolymer/copolymer series in blends and to identify them. Multi-step Mass-remainder analysis can be especially effective for quality control in polymer/copolymer production companies to save time and increase accuracy and precision.

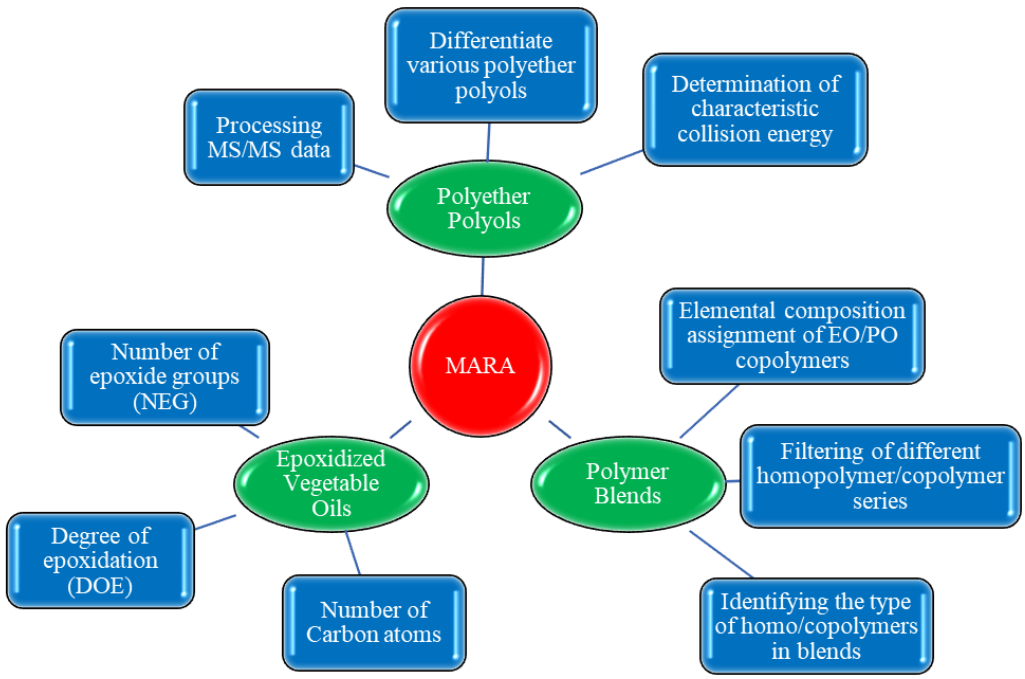

Figure 1 Demonstration of our work plan

Furthermore, we expand our research to investigate the structural characterization of the polyether polyols applying tandem mass spectrometry (ESI-Qq-TOF MS). We examine the multi-arm polyol polymers such as glycerine and sorbitol-based polyether polyols. Developing tandem mass-remainder analysis (TAMARA) allows us to process complex mass spectra and propose a novel method for the distinction of diol, triol and hexaol polyether (co)polymers. We also perform CID experiments to find the characteristic collision voltage for all polyether polyols. Different industrially important copolymers as well as another type of distinctions such as number of heteroatoms, rings or aromatic moieties can be analysed and differentiated by tandem mass-remainder analysis method.

2. LITERATURE REVIEW

2.1 Polymers

2.1.1 Introduction to Polymers

Polymers are macromolecules built up by the attaching covalently together of large numbers of monomers forming polymer molecules. (**Fig. 2**) [1]. Depending on the number of repeating units, polymerization product can be either oligomer or polymer [2,3]. There are two types of polymers: synthetic, which are derived e.g., from petroleum oil (nylon, polyethylene, polyester, polyurethane, PVC etc.) and biopolymers, which derived from living organisms (silk, wool, DNA, cellulose, proteins etc.) [4,5].

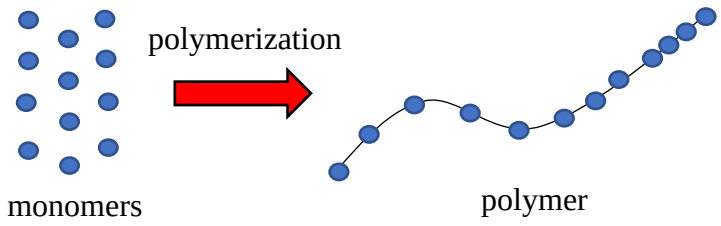

Figure 2 Monomers vs polymer.

Polymers are classified into chain and step-growth polymers (condensation and addition polymers) [6,7] based on polymerization mechanism. **Table 1** demonstrates some important condensation and addition polymers. The most important difference between chain and step polymerizations is the reactivity of the identities of the species with one another. Another difference is the way in which polymer molecular size depends on the extent of conversion **(Fig. 3)**. [8] Living polymerization is a type of chain polymerization where termination of growing polymer chain and chain transfer reactions are suppressed. Growing polymer chains consistently

remain “living” and the molecular weight can easily be controlled. This feature of living polymerization increases its use in several applications [8-10].

Table 1 Condensation and Addition Polymers.

Condensation polymers		Addition polymers	
Polymer	**Characteristic Linkage**	**Polymer**	**Repeating unit**
Polyamide	−NH—CO−	Polyethylene	—CH_2−CH_2—
Polyester	−CO−O−	Polyacrylonitrile	—CH_2−CH(CN)—
Polyurethane	−O−CO−NH−	Poly(vinyl chloride)	—CH_2−CH(Cl)—
Polysiloxane	−Si−O−	Polystyrene	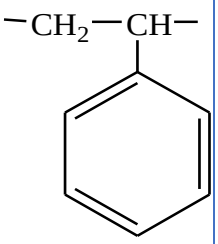
Polyacetal		Polytetrafluoroethylene	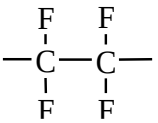

Polymers can further be classified as linear, branched, or crosslinked polymers depending on their structural arrangement. The difference between the shapes of linear and branched polymers molecules can be seen from the structural representations shown in **Figure 4.** Branch points are marked by heavy dots. In crosslinked polymers, polymer molecules are attached to one another at points other than their edge points [8].

Macromolecules can be classified as amorphous, crystalline, or semi-crystalline polymers. Example of crystalline polymers include polyamide, Teflon, PET, PE, PP; while examples of amorphous polymers include ABS, PMMA, PS, PVC [11].

As shown in **Figure 5**, polymers are also classified into thermoplastic and thermosets based on physical properties. Thermoplastics can be reheated, reprocessed, and cooled as necessary without causing any chemical changes, while thermoset plastics remain in a permanent solid state once hardened [12,13].

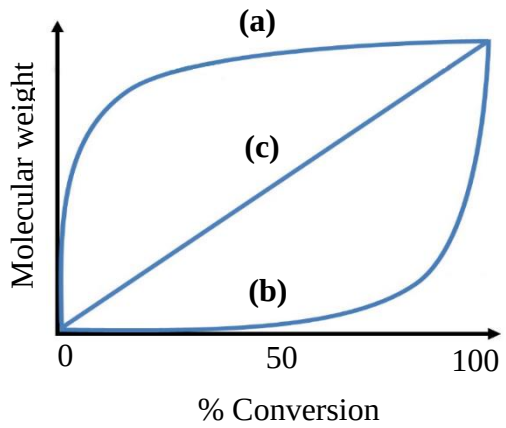

Figure 3 Variation of molecular weight with conversion; (a) chain (b) step and (c) living polymerization.

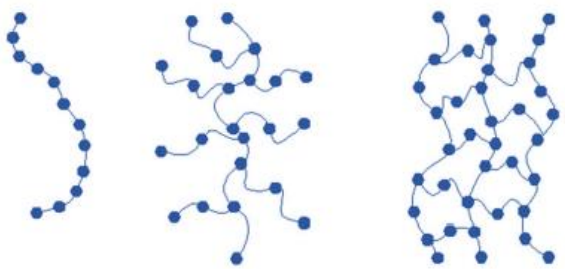

Figure 4 Structure of linear, branched, and crosslinked polymers.

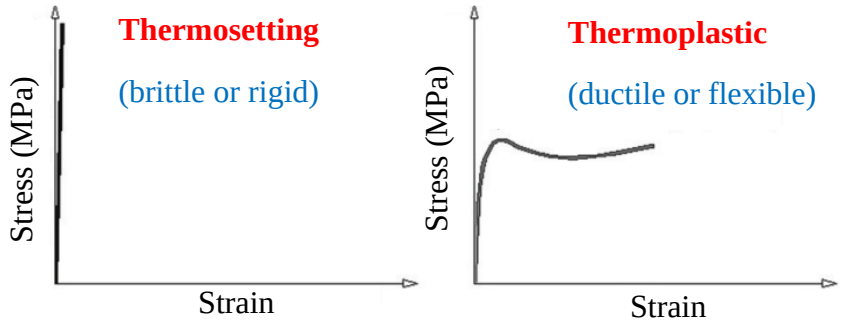

Figure 5 Classification of polymers depending on physical properties.

2.1.2 Polyethers

Polyethers contain ether linkages in the backbone: (R-O-R' where R, R' are alkyl or aryl group). Polyethylene glycol (PEG) and polypropylene glycol (PPG) are simple polyether compounds. They are prepared by ring-opening polymerization (ROP) of ethylene oxide and propylene oxide, respectively. (**Fig. 6**) [14].

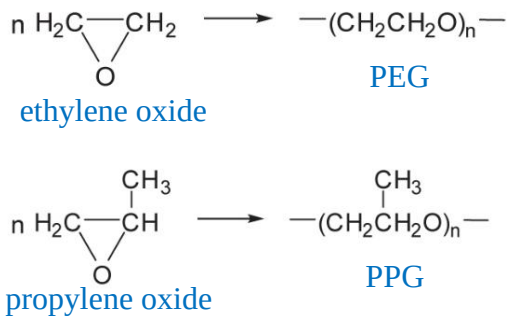

Figure 6 Schematic of PEG and PPG polymerization**.**

PEG has a large variety of applications such as in pharmaceutical, cosmetic, and medical fields and is used for a wide range of products diverging from skin care products to tablet formulations, laxatives, and food additives [15,16]. PPG is used as lubricants, antifoaming agents, softeners, rheology

modifiers, flexible poly(urethane) foams, non-ionic surfactants, wetting agent, and dispersant in leather finishing [17].

2.1.3 Polyether Polyols

Polyether polyols have one or more functional end-groups such as a hydroxyl group. Polyalkylene oxide polyether polyols (**Fig. 7**) are the most important group of polyols for polyurethane (PU) production [18]. Because polyols and di- or polyisocyanates are raw materials for synthesizing of polyurethanes (**Fig. 8**). One of the reasons of this variety of the PU applications arises from the adjustability of the nature of polyols. The essential characteristics, such as the molecular structure and the number of reactive hydroxyl end-groups influence the properties of the final PU product [19]. Therefore, polyurethanes are used in a wide diversity of applications such as flexible and rigid foams, adhesives, coatings, sealants, elastomers, fiber composite materials, paints, etc. [18,20]. PUs are extensively used in the automotive industry in many applications such as cushioning, bumpers, and sound insulation [21,22].

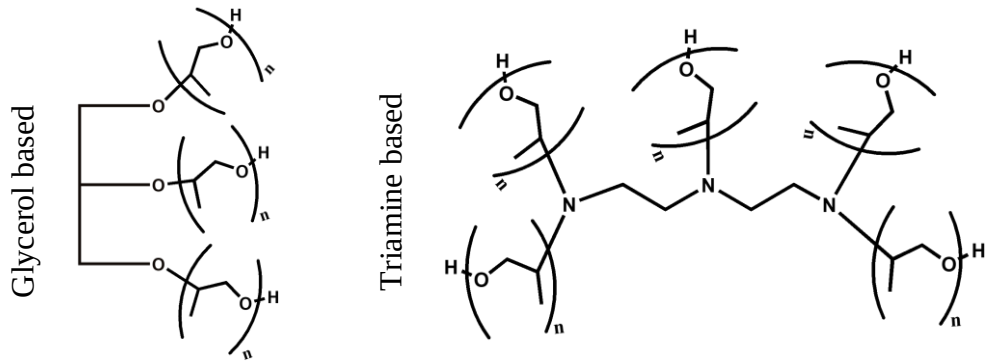

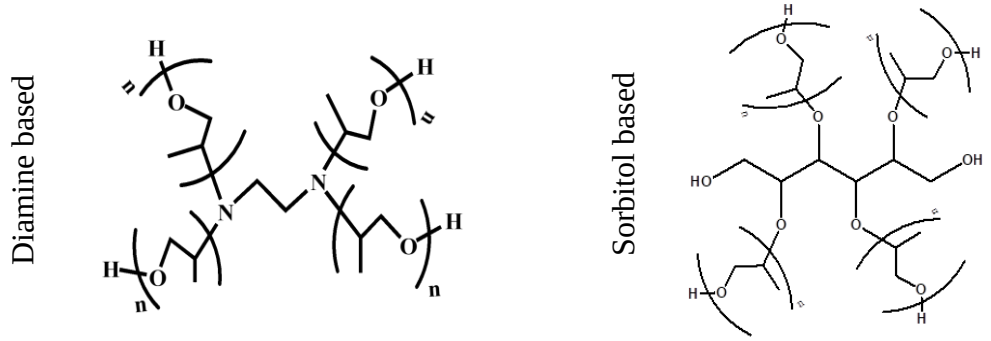

Figure 7 Polyalkylene oxide polyether polyols.

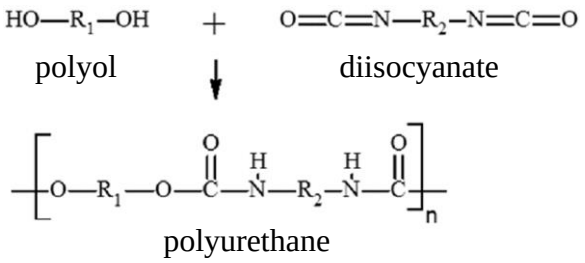

Figure 8 Synthesis of polyurethanes.

2.1.4 Copolymers

A copolymer is a polymer formed when two or more different types of monomers are attached in the main polymer backbone. Copolymers can be categorized based on the arrangement of repeating units as:

Alternative **Random** **Block** **Graft**

In a block copolymer, all monomers aligned in a linear arrangement of blocks and two or more homopolymers linked together in a sequence:

-A-A-A-A-A-B-B-B-B-B-B-A-A-A-A-

In a random copolymer, monomers link in any order [23]:

-A-A-B-B-B-A-B-A-A-B-B-B-A-B-A-A-A-

2.1.5 Poloxamers

Poloxamers are non-ionic triblock copolymers composed of a central hydrophobic chain of PPO flanked by two hydrophilic chains of PEO (**Fig. 9**).

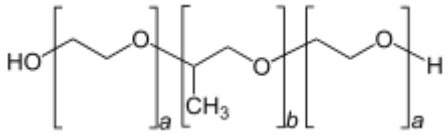

Figure 9 General structure of triblock copolymers.

Triblock copolymers of EO and propylene PO are widely used as non-ionic surfactants in the chemical industry, antifoams and wetting agents in the paper industry, water treatment, fermentation or as a component of machine dish washing mixtures and spray cleaners and novel nonviral vectors in therapeutics for drug and gene delivery. Triblock copolymers can be arranged in an EO-PO-EO or PO-EO-PO sequence. This arrangement results in an amphiphilic copolymer, in which the block sequence and block length determine the properties of the copolymer [24-29].

In our study we worked with Pluronic type triblock copolymers such as PE3100, PE3500, PE8100 and RPE 1740. Pluronic PE 3100 is used to disperse dyes and pigments and employed as an antifoam agent in many applications. PE 3500 is used in formulations for textile appliances. PE 8100 is engaged as a detergent and antifoam in washing and sanitation applications. RPE 1740 is a Pluronic RPE type copolymer. Reverse type block copolymers are flanked by two polypropylene oxide blocks where polyethylene oxide block is in the centre [30,31].

As a random copolymer we used polylactide/polycaprolactone (PLA/PCL) and Rokopol RF551. They are commonly used for biomedical applications due to their biodegradability and biocompatibility, and for

production of polyurethane (PUR) rigid and semi-rigid foam production in reaction with isocyanate, respectively [32,33].

Poloxamers are also used to inhibit multidrug resistance (MDR) proteins and other drug efflux transporters on the surface of cancer cells. MDR proteins are responsible for the drug efflux from the cells and therefore develops the susceptibility of cancer cells to chemotherapeutic agents. Moreover, it has been demonstrated recently that Pluronic can effectively deplete tumorigenic intrinsically drug-resistant cancer stem cells (CSC) [34-37].

2.1.6 Polymer Blends

A polymer blend is a mixture of two or more polymers that have been blended to create new physical properties. Because of an easy and cost-effective method of developing polymeric materials, polymer blending has significant importance in a wide variety of commercial applications [38,39]. Containing different types of copolymers in the blend, the mixture provides materials with better compatibility and develops nanoparticles in drug delivery systems [40-42].

In many consumer-oriented and robust applications, the mechanical strength and thermal properties of polymer blends is the most important aspect. Blend has been reported to have more mechanical and thermal stability than individual polymers [43-46]. Having good dielectric constant values creates further opportunities for blends to be used in electrical industries such as for capacitors [47]. High optical properties of polymer blends allow to use in a wide range of applications ranging from packaging to glazing products in construction and automobile industry [48]. **Figure 10** summaries the main applications of polymer blends.

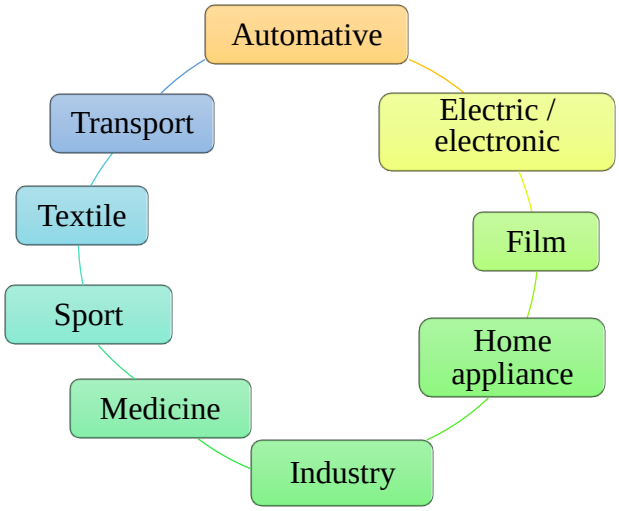

Figure 10 Applications of polymer blends **[49]**.

2.2 Epoxidized Vegetable Oils

Vegetable oils are edible oils extracted from mainly seeds containing triglycerides, i.e., triesters of glycerol with saturated and unsaturated fatty acids (FAs). There are many vegetable oils available such as canola oil, corn oil, olive oil, cottonseed oil, linseed oil, palm oil, rapeseed oil, soybean oil etc. Epoxidized oils are formed by converting of carbon-carbon double bonds in the unsaturated fatty acids into epoxy groups [50], which are non-toxic and can be used in photopolymerization [51,52]. Soybean oil and linseed oil are most popular epoxidized vegetable oils to produce biopolymers. Epoxidized soybean oil (ESBO) is as a green plasticizer used in the production of polyvinyl chloride (PVC) plastics [53,54]. Epoxidized linseed oil (**Fig. 11**) is also used as a plasticizer as well as a toughening agent. [55,56]. With acrylate and urethane derivatives they can be used as surface coatings [57,58] and in ink applications [59,60], respectively.

Applying our method, we determined the fatty acid composition, the degree of unsaturation, the number of epoxide groups per molecule (NEG) and

the degree of epoxidation (DOE, the percentage of conversion from double bonds to epoxide groups) of the epoxidized soybean and linseed oils.

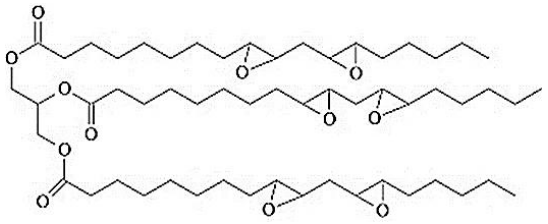

Figure 11 Structure of epoxidized linseed oil.

Triglyceride oils were previously characterized with different methods such as infrared spectroscopy, particularly Fourier transform infrared (FTIR) spectroscopy, gas chromatography–mass spectrometry (GC-MS), nuclear magnetic resonance (NMR) spectroscopy and electrospray ionization mass spectrometry (ESI-MS) [61-63].

2.3 Mass Spectrometry

2.3.1 Introduction to Mass Spectrometry

Mass spectrometry (MS) is one of the analytical techniques used in characterization of polymers with a high range of molecular mass. It simply measures the mass-to-charge ratio of ions. Obtained plot is called a mass spectrum representing intensity on the y-axis and mass-to-charge ratio (m/z) on the x-axis.

New era to mass spectrometry started by J.J. Thompson in 1897 [64]. A couple of year first isotopes were observed by Aston F.W with MS. [65] Detection of trace biomolecules was possible after invention of accelerator mass spectrometry in 1939 [66]. Time-of-Flight (TOF) and Ion Cyclotron Resonance (ICR) mass analysers were the beginning of ultra-high resolution mass spectrometry [67,68]. There are other important techniques such as Quadrupole [69], Fourier Transform Ion Cyclotron Resonance (FTICR) [70]

and Orbitrap analysers [71] and Electrospray Ionisation (ESI) [72] Atmospheric Pressure Chemical Ionisation (APCI) [73] and Matrix-Assisted Laser Desorption Ionization (MALDI) [74] ionization methods which are used to study biological samples, proteins, peptides as well as oligonucleotides and nucleic acids.

Mass spectrometer mainly consists of three parts: an ion-source, a mass analyser, and a detector. Ions are formed in an ion source by ionising the molecules. There are many types of ionization techniques, depending on the sample phase (solid, liquid, gas). After ionization, ions travel through the mass analyser into the detector. Mass analyser sorts the ions according to their m/z values. **Figure 12** shows schematics of a mass spectrometer.

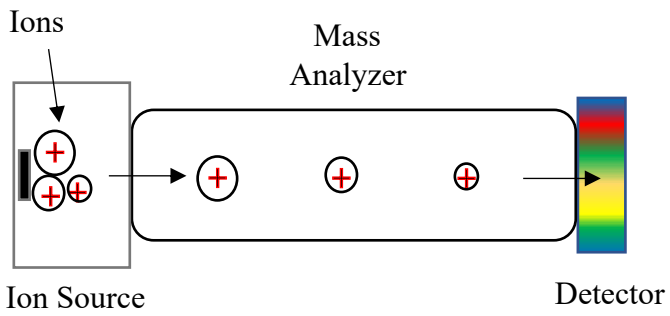

Figure 12 Schematic diagram of a mass spectrometer.

2.3.2 Ion Sources

Introductory part of the mass spectrometer is called ion-source where samples are ionised and sent to mass analyser to be separated and measured [75]. Depending on the degree of excitation during ionization techniques ion-sources are divided into two groups: soft and hard ionization techniques. Example for hard ionization method is the Electron Ionization (EI) [76]. Sample is thermally vaporized in high vacuum and ionized by collision with

an electron beam. This method produces many extensive fragmentations - molecular radical cations. In soft ionization method it produces ions of the molecular species such as matrix-assisted laser desorption ionization [77], electrospray ionization [78], atmospheric pressure ionization (API) [79] etc. **Figure 13** displays general overview of ionization methods.

In our experiments we used MALDI and ESI ionization sources. We will concentrate on the working principles of these two ion-sources.

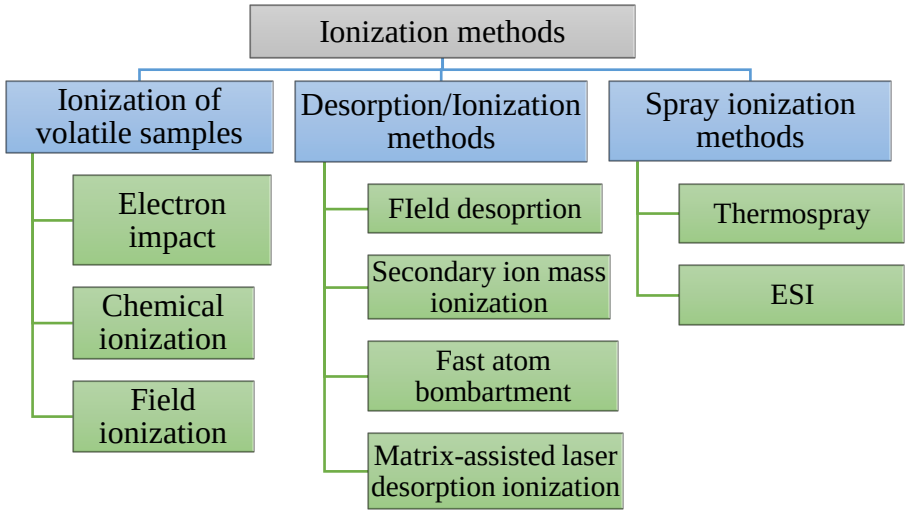

Figure 13 Classification of the Ionization methods.

One of the soft ionization methods is the MALDI, which was introduced by Karas and Hillenkamp [80,81]. Japanese scientist Tanaka Koichi received the Nobel Prize for Chemistry in 2002 for developing technique to identify and analyse proteins and other large biological molecules [82]. In a short time, it became a well-known and robust instrument as it produces intact gas-phase ions from non-volatile and thermally labile compounds. Another benefit of this method is the easy sample preparation and large tolerance to contamination by salts. [83] Samples are dissolved and mixed with the matrix solution. Depending on the nature of samples, different matrices (**Table 2**) can be selected. Matrices should absorb the laser light

(**Table 3**). Our MALDI-TOF instrument is equipped with a 355 nm pulsed UV laser. Very small amount of the sample is dropped onto the MALDI plate and let it dry [84]. Then the plate is introduced into the ion-source under vacuum. In some seconds particular portion of the sample can be ablated by laser pulses.

Table 2 Common MALDI matrices.

Analyte	Matrix
Peptides/proteins	2,5-Dihydroxybenzoic acid (DHB) 3,5-Dimethoxy-4-hydroxycinnamic acid (SA)
Oligonucleotides	Trihydroxyacetophenone (THAP)
Carbohydrates	2,5-Dihydroxybenzoic acid (DHB) Trihydroxyacetophenone (THAP)
Synthetic polymers	Dithranol (DIT) 2,5-Dihydroxybenzoic acid (DHB)
Organic molecules	2,5-Dihydroxybenzoic acid (DHB)
Inorganic molecules	Trans-2-(3-(4-tert-Butylphenyl)-2methyl-2-propenyliedene)malononitrile
Lipids	Dithranol (DIT)

Table 3 Common lasers used for MALDI**.**

Laser	Wavelength
Nitrogen	337 nm
Nd:YAG µ3	355 nm
Nd:YAG µ4	266 nm
Er:YAG	2.94 µm
CO_2	10.6 µm

Figure 14 displays the schematic of the MALDI. The rapid absorption of the photons and thereby heating causes desorption of the ions and expansion of them into the gas phase. The ions in the gas phase are then accelerated by a voltage gradient towards the mass analyser [85].

Under MALDI conditions mainly singly charged adduct ions are formed. Being soft ionization method, MALDI produces singly charged adduct ions. There are two types of fragmentation may happen under MALDI conditions. Fragmentation can occur in the ion-source (in-source decay, ISD) and after the acceleration region, which is called post-source decay (PSD), respectively.

There are some shortcomings of MALDI such as having low shot-to-shot reproducibility and strong dependence on the sample preparation. Laser shot ablates a few layers of the portion at the spot causing variation in the shot-by-shot spectrum. Homogeneous sample gives a better reproducibility of the signal.

Electrospray ionization (ESI) was introduced by Fenn et al. [86]. Unlike MALDI, ESI produces multiple charged ions. It is a soft ionization method and suitable for analysis of protein, polymers, biopolymers as well as small polar molecule. One of the technical advantages of ESI is that it can be coupled with HPLC and capillary electrophoresis. This feature extends its application in different areas [87-89].

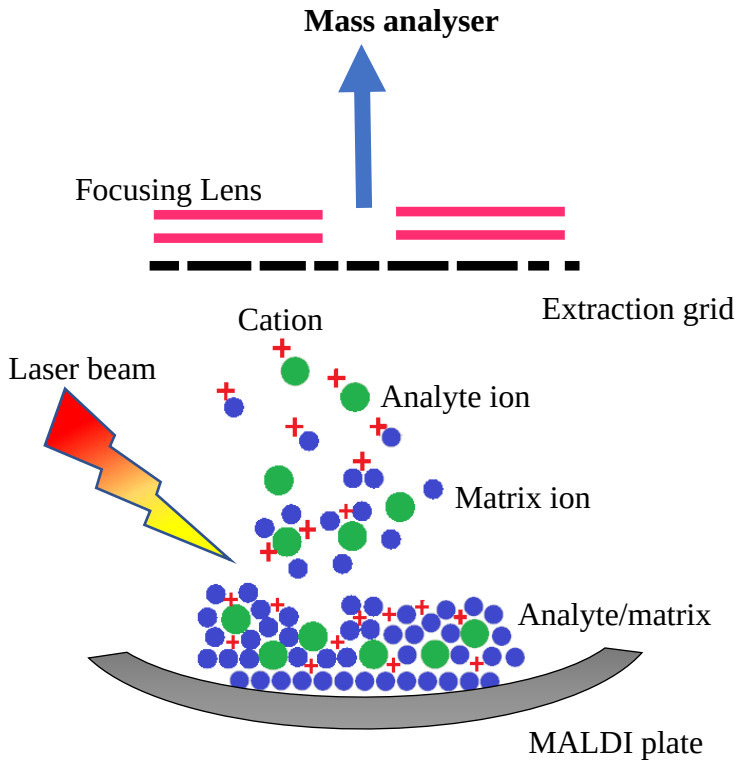

Figure 14 Schematic of MALDI process.

ESI occurs under strong electric field and atmospheric pressure. As a liquid sample passing through a capillary tube, because of a potential difference between this capillary and the counter-electrode, results in forming highly charged droplets (**Fig. 15**). These droplets then go through inert gas "curtain" to remove solvent molecules.

Because of some electrochemical process happens at the probe tip, multiply charged ions can be formed from high-molecular-weight molecules such as proteins. This is another advantage of ESI. This feature increases the sensitivity, and it makes possible to measure large molecules with low mass limit analysers [90].

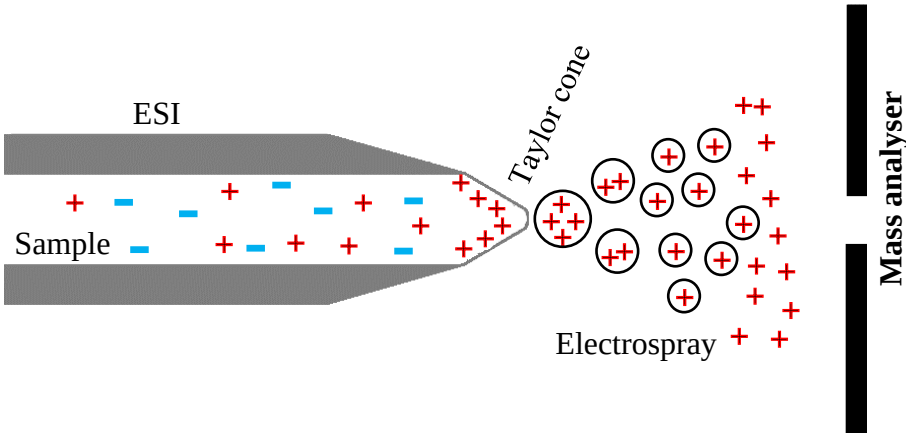

Figure 15 Mechanism of electrospray ionization process**.**

There are some disadvantages of ESI e.g., the experimental parameters should be carefully chosen; not all the solvents can be used with ESI; there are always fluctuations in the signal [91].

ESI is the best ionization source for high polarity, thermally unstable proteins. ESI can be used in the analysis of proteins, metabolites, peptides, and nucleotides [92-94].

2.3.3 Mass Analysers

Mass analyser is the heart of mass spectrometer, in which mass/charge separation occurs. There are several types of mass analysers. **Table 4** demonstrates the types and main parameters of the mass analysers.

In our studies we worked with TOF and Quadrupole type mass analysers and thus we will discuss them in detail. Quadrupole is a mass analyser, which uses the stability of the trajectories in oscillating electric fields to separate ions according to their m/z ratios.

Table 4 Characteristics of mass spectrometers [95].

Mass Analysers	Mass limit	Resolution	Accuracy	Ion Sampling	Pressure (Torr)
Quadrupole	4000 Da	2000	100 ppm	continuous	10^{-5}
Ion trap	6000 Da	4000	100 ppm	pulsed	10^{-3}
TOF	>1000 000 Da	5000	200 ppm	pulsed	10^{-6}
TOF reflectron	10 000 Da	20000	10 ppm	pulsed	10^{-6}
Magnetic	20 000 Da	100000	<10 ppm	continuous	10^{-6}
FTICR	30 000 Da	500000	<5 ppm	pulsed	10^{-10}
Orbitrap	50 000Da	100000	<5 ppm	pulsed	10^{-10}

Quadrupole analysers are made up of four perfectly parallel rods of circular section **(Fig. 16)**. Positive charged ion enters between the rods then moves towards a negative rod [95,96]. As ions moving along the z axis, the effect of a total electric field lays over on a constant current resulting potential applied (Φ_0) to the rods:

$$\Phi_0 = +(U - V \cos \omega t) \text{ and } -\Phi_0 = -(U - V \cos \omega t) \quad (1)$$

In Eq (1) equation, ω represents the angular frequency, U is the direct potential, V is the amplitude of the RF voltage and (V cos ωt) is radiofrequency. When positive ions move closer a positive rod, the potential energy increases. Conversely, it decreases if ions move towards a negative rod. But the alternative field turns the potentials, alternating up and down. If the frequency is high enough, an ion moves down the towards a negative rode is trapped in the lower positive potential curve and is thus brought back to the centre of the quadrupole rods [97].

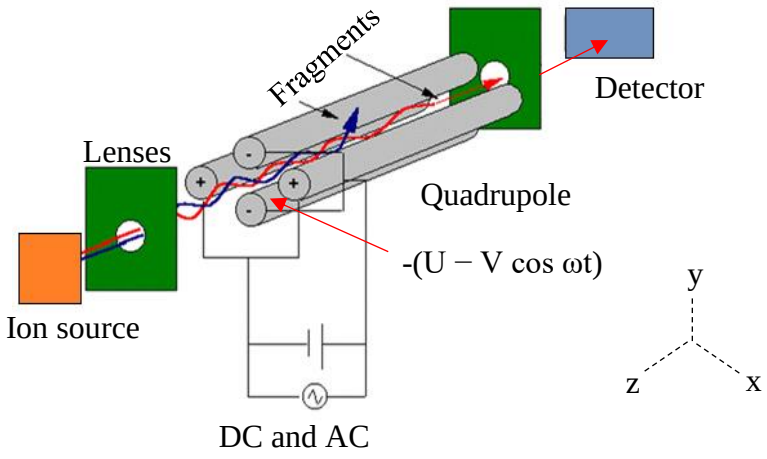

Figure 16 Schematic diagram of a quadrupole analyser.

Mass spectrometers with quadrupole analyser are extensively used where a specific group of ions are being studied because they can stay focused on a single ion for extended period. This is useful in LC-MS or GC-MS where they serve as high specificity detectors. Quadrupole is at reasonable cost and multi-purpose instrument. The single quadrupole MS with EI is used as a standalone analyser in residual gas, and real time gas analysers, plasma diagnostics and SIMS surface analysis systems [98].

Another mass analyser is time-of-flight (TOF) where mass-to-charge ratio of each ion is determined by a time-of-flight measurement. Stephens described the TOF analysers for the first time in 1946. [99] Then it was developed by different scientists to broaden the application of TOF analysers [100-104].

They can be used in linear and reflectron modes. Linear mode is suitable with much higher molecular weight samples, but the reflectron mode results in the high resolution as well as more accurate mass determination which is important for proteomics and other biological measurements [105].

Figure 17 demonstrates the scheme of a linear TOF analyser. The TOF instrument separates ions according to their time of flight when they move in a flight tube. Before this, all ions are accelerated by electric field and driven out from the source. Because of potential gradient applied between an electrode and the extraction grid ions are forced towards the flight tube. It makes all ions have the same kinetic energy. After quitting the drifting region, ions move towards a field-free region where they are separated according to their speeds. Lighter ions move in much higher speeds and reach the detector first. As an ion with m mass and ze charge leaves the source, accelerated by a potential Vs. Its electric potential energy E_{el} is transformed into kinetic energy E_k Eq (2):

$$E_k = \frac{mv^2}{2} = qV_S = zeV_S = E_{el} \tag{2}$$

The speed of the ion leaving the source is given by Eq (3):

$$v = (2zeV_S/m)^{1/2} \tag{3}$$

The time needed to reach detector through the distance L is given by Eq (4):

$$v = \frac{L}{v} \tag{4}$$

Replacing V by its value in Eq (4) gives Eq (5):

$$t^2 = \frac{m}{z}\left(\frac{L^2}{2eV_S}\right) \tag{5}$$

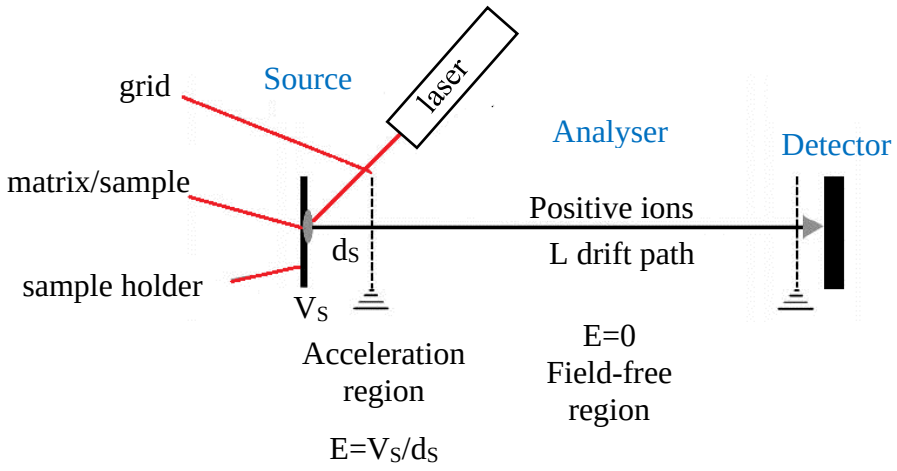

Figure 17 Schematic diagram of a linear TOF analyser.

Using Eq (5) we can calculate m/z from a measurement of t^2 where parenthesis inside is constant. This equation also shows that an ion with lower mass will reach the detector faster.

Replacing V by its value in Eq (4) gives Eq (5):

$$t^2 = \frac{m}{z}\left(\frac{L^2}{2eV_S}\right) \tag{5}$$

It is very important to mention the delayed extraction mode (DE) used in TOF measurements. Because in continuous extraction mode the same mass ions initially with higher kinetic energy reach detector faster than the same mass ions initially with lower kinetic energy. Thus, it causes broadening of the peaks. It results a decrease in resolution. But in delayed extraction mode ions are first separated based on their initial kinetic energy in the field free region of the ion-source as in continuous extraction mode, then applying voltage pulse to the ions (delayed extraction). Thus, ions stayed for a longer time in the source gain more kinetic energy, and they reach the detector at the same time with the ion, which had initially higher kinetic energy. This mode

significantly improves the resolution of the TOF analysers. **Figure 18** displays schematic description of the delayed extraction mode in a linear TOF analyser [106].

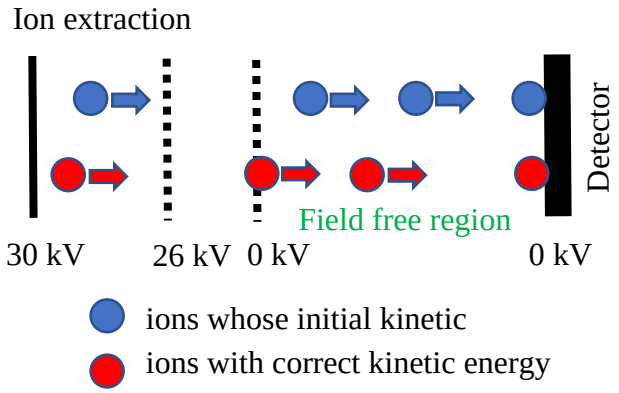

Figure 18 Schematic diagram of the delayed pulsed extraction a linear TOF analyser.

In addition to delayed extraction, reflectron introduced by Mamyrin can also be used to improve the resolution of the mass analysers [107]. This is called reflectron time of flight (RTOF) analysers**.** Reflectron decreases a spread of flight time of the same m/z ions and corrects the kinetic energy dispersion of the ions. Because the ions with higher speed penetrate reflectron more deeply and spend more time in the reflectron resulted in that all ions reach the detector at the same time (**Fig. 19**). Another advantage of the reflectron is that it extends the flight path without increasing the dimension of the mass analyser. Reflectron increases the mass resolution and mass accuracy. **Fig. 20** shows the single stage reflectron, which consists of 38 ring electrodes connected to resistors.

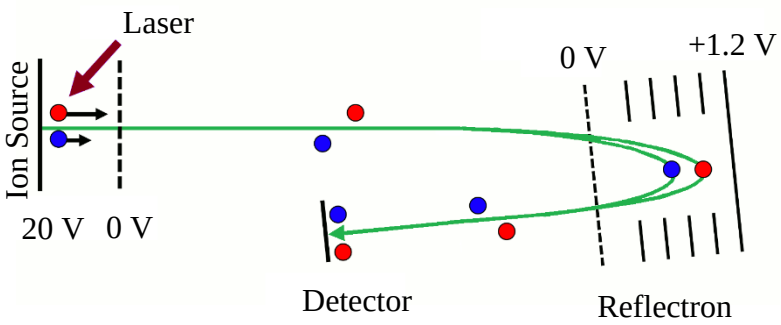

Figure 19 Schematic diagram of the reflectron.

Figure 20 Single stage reflectron [108].

2.3.4 Detectors

A last element of mass spectrometers is the detector that converts the current of separated ions into measurable signal. Different types of detectors are used based on the charge, mass or velocity of the ions as well as suitability to the mass analyser. The most common types of ion detectors are Faraday cup, electron multiplier, electro-optical ion detector and photomultipliers.

The simplest and cheapest detector is Faraday cup where incident ions hit the dynode surface causing emission of the electrons and the resulting in a potential drop across the resistor, which is amplified and recorded [109]. In a

photomultiplier, electrons, which emitted by strike of ions from dynode, hit a phosphorous screen resulting burst of photons. The photons then move into the multiplier where amplification takes place [110]. The electro-optical ion detector comprises of ion and photon detection parts. These detectors coverts ions to electrons and then to photons [111].

Our ESI-QTOF and MALDI-TOF instruments are equipped with microchannel plate (MCP) detectors (well-suited to TOF analysers). MCP is one type of continuous dynode electron multipliers besides discrete dynode electron multipliers. It is a circle plate in which parallel cylindrical channels were punched (**Figure 21**). It amplifies particles by the multiplication of electrons via secondary emission because each channel is covered by semiconductor element. Therefore, having many channels, which are parallel to each other, the microchannel plate detector provides spatial resolution. Channels are 10 μm in diameter and inclined at a small angle of 8° to the MCP surface.

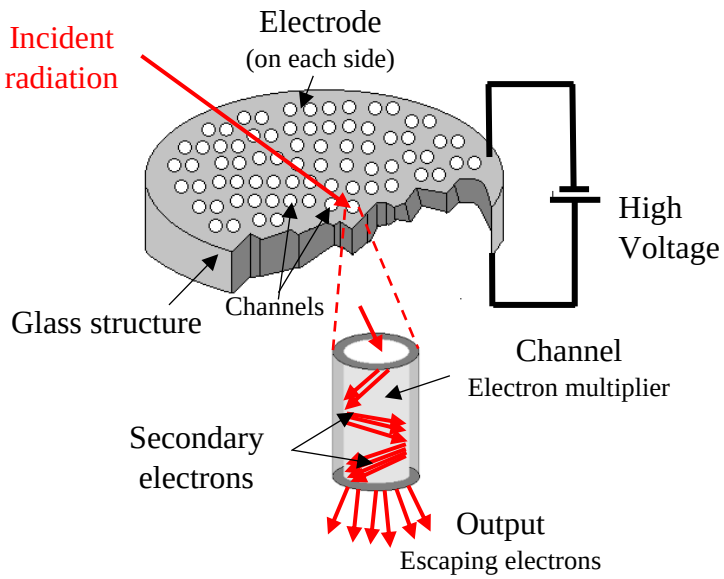

Figure 21 Schematic diagram of the operation of a microchannel plate.

The disadvantages of microchannel plate detectors are being fragile, sensitive to air and expensive [112-116].

2.3.5 Tandem Mass Spectrometry

A tandem mass spectrometer (MS/MS) usually uses two mass analysers to provide information on the structure of the molecules [115,116]. In the first step, analyser isolates the precursor ion and because of some activation energy, product ions may be formed. In the second step, ions collide with gas molecules (mostly N_2) resulting in fragmentation by collision-induced dissociation (CID) [116,117]. The extent of fragmentation can be given by survival yield (SY).

$$SY = \frac{I_p}{I_p + \sum I_{F,i}} \tag{6}$$

where I_p is intensity of the product ion, $\sum I_{F,i}$ is a sum of all fragment ion intensities [120].

CID takes place in two steps: the excitation of the precursor ions and unimolecular dissociation of an excited ion, separation of the fragment ion, consequently. The collision between precursor ion and collision gases increases the internal energy of the precursor ion and the increase in the internal energy is distributed among the different vibrational degrees of freedom. Thus, a precursor ion can decompose into several product ions in collision-induced dissociation [90,120].

In our measurements we used Qq-TOF MS instrument (**Fig. 22**). The Qq means an instrument with two quadrupoles where lower-case q is the reaction region. It operates in RF-only as collision cell. This is combined with TOF analyser. The TOF analyser then sorts the fragments produced from the analyte. In addition to CID there are other ways for ion-activation such as

electron capture dissociation (ECD), electron transfer dissociation (ETD) etc [121,122].

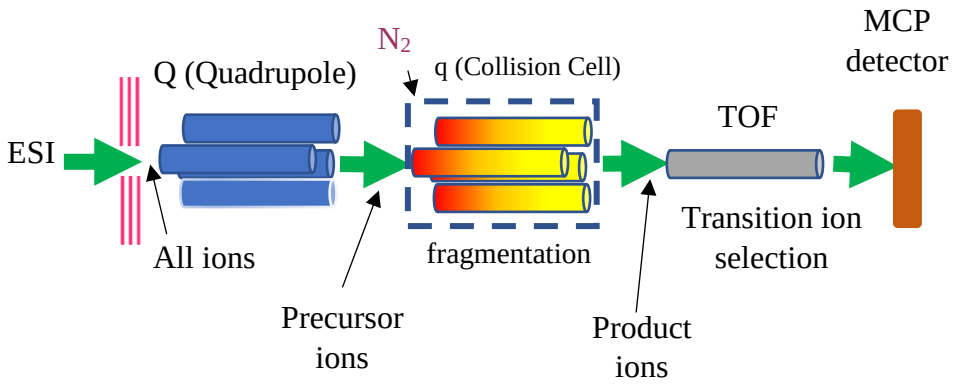

Figure 22 Schematic diagram of the Qq-TOF MS instrument.

There are four scan modes (precursor ion scan, product ion scan, neutral loss scan, and selected reaction monitoring) which are used in triple quadruple (QQQ) tandem mass spectrometry. In a precursor ion scan, first the fragments are selected in the second mass analyser, then precursor ions are scanned in the first analyser. In a product ion scan, a precursor ion with known m/z value is selected in the first step, being fragmented and then all masses are scanned in the second mass analyser. In a neutral loss scan both analysers are scanned continuously. The first mass analyser scans all the masses while the second mass analyser sets an offset, which relates to a neutral loss with the mass of the desired neutral. Last scanning mode is selected reaction monitoring. Depending on the number of product and precursor ions, single reaction monitoring (SRM) or multiple reaction monitoring (MRM) are applied [123,124]. There are some important applications of tandem mass spectrometry such as elucidation of structure, determination of fragmentation

mechanisms, determination of elementary compositions, kinetics studies, etc [125-127].

2.4 Mass-Remainder Analysis (MARA)

In our studies we measured polymers and a huge number of m/z peaks arising from different homopolymer/copolymer series as well as different types of epoxidized oils was detected. Because of the complex spectrum, i.e., the presence of many peaks, evaluation of each peak is very time-consuming (it can take hours or even days). To shorten the analysis time, we applied the recently invented data mining method - Mass-Remainder Analysis (MARA) [128]. Using this method, we were able to determine the copolymer composition from complex mass spectra and also from different epoxidized triglyceride mass spectral peak series, and the number of carbon atoms and epoxide groups within a short time. Using Eq (7) we can calculate Mass-Remainder values of the measured m/z peaks:

$$MR = m/z - int\left(\frac{m/z}{R}\right) * R \tag{7}$$

where R is the exact mass of the repeating unit (i.e., C_3H_6O = 58.04187 Da) and int(x) rounds x down to the nearest integer. MARA uses 4 main steps:

1. Calculation of the Mass-Remainder values
2. Determination of number of monomer units
3. Correction of overlapped peaks
4. Summing isotope peak intensities

Referring to [129], we developed this data mining procedure to be able to handle the complex mass spectra of polymer blends containing copolymers and to apply it for tandem mass spectrometric measurements to gain structural information. This method can handle m/z values from moderate/low resolution complex mass spectra. MARA does not require high accuracy and well-separated peaks.

There are also other data processing and visualization methods such as Kendrick mass defect [130], van Krevelen [131] and Resolution-Enhanced KMD analyses [132]. Therefore, these methods require transformation to a new mass scale and higher mass accuracy to prevent any distortion in the visual analysis of the complex mass spectra when filtering for particular compounds.

The advantage of our method is that it is not based on the calculation of mass defect but on the calculation of the remainder after dividing by the exact mass of one of the repeat units of the copolymer. Moreover, because of deisotoping ability, MARA can analyse much more complex spectra of various copolymers recorded by a MALDI-TOF mass spectrometer. MARA also deals with the overlapped peaks of the different copolymers.

3. EXPERIMENTAL SECTION

3.1 Chemicals

The epoxidized triglyceride oils were obtained from Arkema (Colombes, France). The samples were dissolved in HPLC-MS grade methanol purchased from VWR International (Leuven, Belgium).

The PE3500, PE3100, PE8100 and RPE1740 EO/PO block copolymers were received from BASF (Ludwigshafen, Germany).

The Rokopol RF551, RF4855 and G1000 polymers were purchased from PCC Group (Brzeg Dolny, Poland). PEG600 and PPG1000 polymers were received from BASF (Ludwigshafen, Germany), Merck (Darmstadt, Germany), and Sigma Aldrich (Steinheim, Germany), respectively. Methanol (HPLC-MS grade) was received from VWR International (Leuven, Belgium).

3.2 Instruments

3.2.1 MALDI-TOF MS

The MALDI-TOF MS measurements of epoxidized oils and polymer blends were carried out with a Bruker Autoflex Speed mass spectrometer (Bruker Daltoniks, Bremen, Germany) equipped with a time-of-flight (TOF) mass analyser. In all cases, 19 kV (ion source voltage 1) and 16.65 kV (ion source voltage 2) were used. For reflectron mode, 21 kV and 9.55 kV were applied as reflector voltage 1 and reflector voltage 2, respectively. A solid phase laser (355 nm, ≥100 μJ/pulse) operating at 500 Hz and 200 Hz was applied to produce laser desorption and 15,000 shots and 10 000 shots were summed for epoxidized oils and polymer blends measurements, respectively.

3.2.2 ESI-QTOF MS

A Maxis II type Qq-TOF MS instrument (Bruker Daltoniks, Bremen, Germany) equipped with an Apollo II electrospray ion source was used. The spray voltage was 4.5 kV. The resolution of the instrument was 40,000 at m/z 400 (FWHM), and the mass accuracy was <2 ppm (external calibration). N_2 was utilized as the drying gas (200 ◦C, 4.0 L/min), nebulizer gas (0.5 bar) and collision gas. The mass spectra were recorded by means of a digitizer at a sampling rate of 2 GHz. The spectra were calibrated externally by ESI tune mix, from Bruker. The spectra were evaluated with the Compass Data Analysis 4.4 software from Bruker (Bremen, Germany). The sample solutions were introduced directly into the ESI source with a syringe pump (Cole-Parmer Ins. Co., Vernon Hills, IL, USA) at a flow rate of 3 μL/min. The concentration of the samples was 0.01 mg/mL. The collision voltage was varied in the range of 20–90 eV and 50-130 eV for epoxidized oil and polyether polyol measurements, respectively.

3.3 Sample Preparation

PLA/PCL random copolymer was synthetized in our lab. DL-lactic acid (88%-92%) from Reanal (Budapest, Hungary) and ε-caprolactone (97%) from Sigma Aldrich (Taufkirchen, Germany) were used. The synthesis was carried out in a 50 mL flask stirred continuously with constant nitrogen bubbling. The temperature was 140°C (oil bath) and vacuum was utilized to facilitate water elimination. The ratio of the monomers was 2:1 lactic acid:ε-caprolactone, respectively. The investigated samples are listed in **Table 5**.

Table 5 List of investigated copolymers and blends.

Name	Component(s)	Composition	M_n (MS) (g/mol)	Type
Sample 1	PE3500	single	1390	block
Sample 2	PLA/PCL	single	640	random
Sample 3	PLA/PCL-PE3100	14:3	740	random-block
Sample 4	RF551-PE3100	1:10	850	random-block
Sample 5	PE8100	single	2720	block
Sample 6	RPE1740-PE8100	1:1	2670	block-block
Sample 7	RF551	single	760	random
Sample 8	PE3100	single	1000	block
Sample 9	RPE1740	single	2360	block

Table 6 demonstrates the composition, structure, and number average molecular weight (M_n) of various types of polyether polyols.

Table 6 List of the investigated polyether polyols.

	Name	Composition	Initiator	Structure	M_n (MS) (g/mol)
Sample 10	PEG600	EO		diol – linear	600
Sample 11	PPG1000	PO		diol – linear	1000
Sample 12	PE3100	EO/PO		diol – linear	1000
Sample 13	G1000	PO	glycerol	triol – 3 arms	1000
Sample 14	RF4855	PO	sorbitol	hexaol – 6 arms	600
Sample 15	RF551	EO/PO	sorbitol	hexaol – 6 arms	800

The MALDI-TOF MS spectra of epoxidized oils were internally calibrated with a mixture of α-,β-,γ-cyclodextrin, rutin and lactose octaacetate. The matrix used for the MALDI-TOF MS was 2′,4′,6′-trihydroxyacetophenone (THAP), dissolved in methanol at a concentration of 20 mg/mL. The epoxidized oils were also dissolved in methanol at a concentration of 10 mg/mL. Sodium trifluoroacetate was used as the ionizing agent (5 mg/mL). The mixing ratio was 50/10/5/2 (matrix/oil/cationizing agent/internal standard mixture). A volume of 0.25 µL of the solution was deposited onto a metal sample plate and allowed to air-dry.

The MALDI-TOF MS spectra of polymer blends were internally calibrated. The samples were mixed with polyethylene oxide homopolymers (PEO). After internal calibration individual calibrant series were created for all samples. These series were applied for internal calibration. The samples were prepared with 2,5-dihydroxybenzoic acid (DHB) dissolved in methanol at a concentration of 20 mg/mL, the blend samples were also solved in methanol (concentration: 10mg/mL). Sodium trifluoroacetate solution were utilized as ionizing agent (concentration: 5 mg/mL in methanol). The matrix, sample and the ionizing agent solutions were mixed in the ratio of 5:2:1, respectively.

All polyether polyols were dissolved in methanol at a concentration of 0.01 mg/mL. Lithium chloride (Sigma Aldrich, Steinheim, Germany) was used as an ionizing agent (4 mg/mL). 10 µL of ionizing agent was added to each of 1 ml-polymer samples, then injected into the ESI-QqTOF MS instrument.

4 RESULTS AND DISCUSSION

4.1 Determination of polymer quantities of the epoxidized soybean and linseed oils

Having information about polymer quantities of the epoxidized oils such as the average number of epoxide groups and the degree of epoxidation (DOE) is very important in designing and production of vegetable oil-based biopolymers. To be able to calculate these values, following steps were done.

First, the epoxidized soybean (**Fig. 23**) and linseed oils (**Fig. 24**) were measured with MALDI-TOF MS. All peaks are the sodium adducts of the epoxidized triglycerides (ETGs). The number of carbon atoms and epoxide groups are indicated in green, respectively. For example, (55:2) peak at m/z 913 equals to the $[C_{55}H_{102}O_8 + Na]^+$ adduct ion with a theoretical m/z 913.7467. The number of carbon atoms and epoxide groups of this ion indicate the chemical formula of this epoxidized triglyceride are as followings:

$$C_3H_8[CO_2(CH_2)_{15}(CHOCH)_1]_2[CO_2(CH_2)_{15}] \text{ or}$$
$$C_3H_8[CO_2(CH_2)_{17}][CO_2(CH_2)_{13}(CHOCH)_2][CO_2(CH_2)_{15}]$$

The chemical composition above reveals that the epoxidized FA contains oleic, oleic, palmitic or stearic, linoleic, palmitic acids, respectively. CO_2 and CHOCH express the carboxyl groups of the fatty acid and the number of epoxy groups, respectively.

In **Figures 23** and **24** blue peaks demonstrate two peaks are very close to each other. For example, there are two peaks with 55 carbon atoms and 5 epoxide groups and 57 carbon atoms 3 epoxide groups at m/z 955 Da in both epoxidized soybean and linseed oils and also 55 carbon atoms and 6 epoxide groups and 57 carbon atoms and 4 epoxide groups at m/z 969 Da in epoxidized

linseed oil. It is because of the replacement of two CHOCH (the epoxy group) groups by six CH_2 groups, which results in a difference of 0.0728 Da. Furthermore, it is important to select the instrument with enough resolution to separate these peaks. At least 13700 resolving power ($m/\Delta m_{50\%}$) at m/z 1000 is necessary to separate these adjacent peaks. Red peak in each spectrum demonstrates the internal calibrant which is a mixture of α-,β-,γ-cyclodextrin, rutin and lactose octaacetate. In the following paragraphs we explain how to sort and easily find all necessary data for vegetable oils.

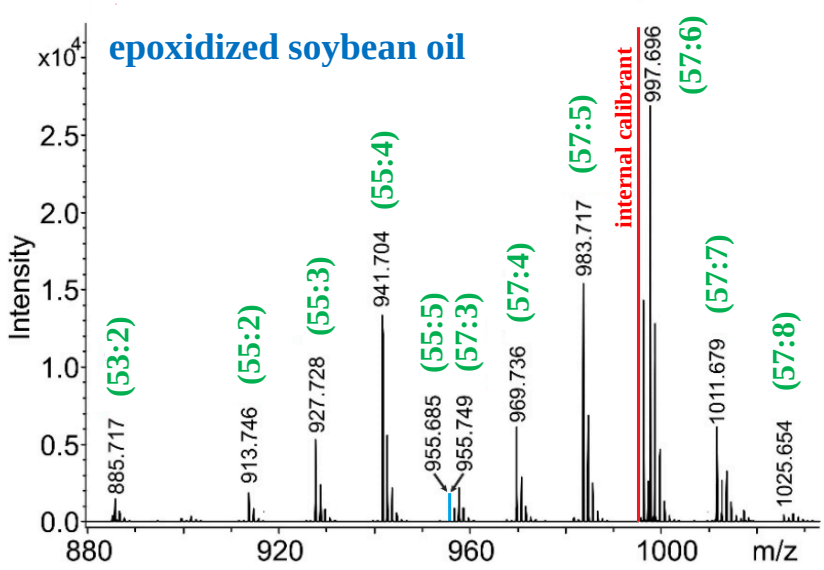

Figure 23 MALDI-TOF mass spectrum of the epoxidized soybean oil.

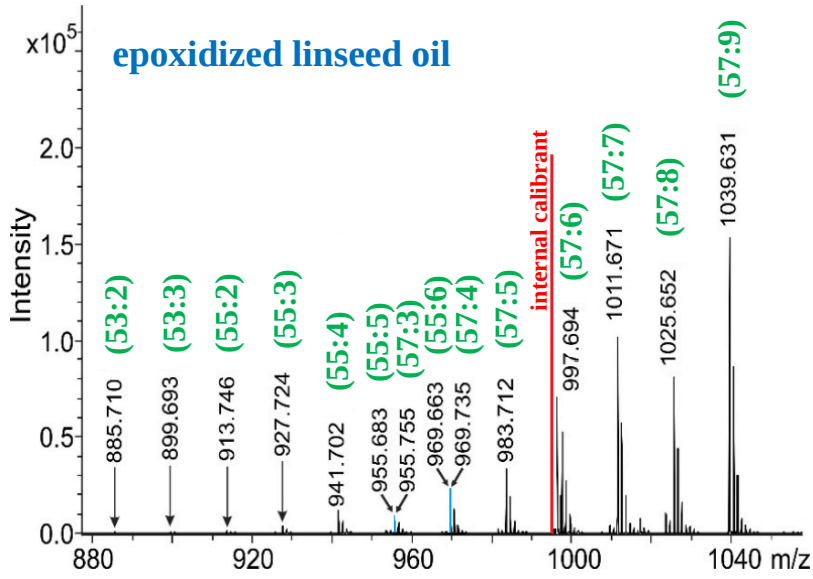

Figure 24 MALDI-TOF mass spectrum of the epoxidized linseed oil.

At first glance mass spectra of the epoxidized oils in **Figures 23 and 24** seem to be very simple. Therefore, there are many peaks with lower intensity such as double bonds (or epoxide groups), CH_2 groups as well as side products such as diols which can be formed by the addition of water in epoxidation reaction. To handle this complex system, we use mass-remainder analysis formula Eq (8) to find mass remainder (MR) values of all peaks.

$$MR = m/z \; MOD \;\; B \tag{8}$$

where B is the exact mass of a base unit and the modulo (MOD) operation finds the remainder after the division. Choosing CH_2 group as a base unit we plot mass-remainder *versus* m/z. In this case, the components (dots) on the same horizontal line in **Figure 25** have the same mass remainder (MR) values but different number of CH_2 groups.

After obtaining all MR values from the spectrum of the epoxidized soybean oil (**Fig. 23**) using Eq (8), we make MR *versus* m/z plot (**Fig. 25**).

Yellow dots are identified and corresponding peaks to epoxidized oils. We can easily observe the triglycerides with one remaining double bond (green highlight), the epoxidized triglycerides (red highlight) and diol side products (blue highlight). The manual evaluation of each peak/series in the mass spectrum is not easy and effective. Because of many peaks with lower intensities, it takes a long time to elucidate the spectrum. Therefore, we use the advantage of MARA method to sort these components into classes based on their MR values. The other dots in grey do not belong to any identified series, most of those are isotopic peaks. Size of the dots expresses the relative intensity of each peak.

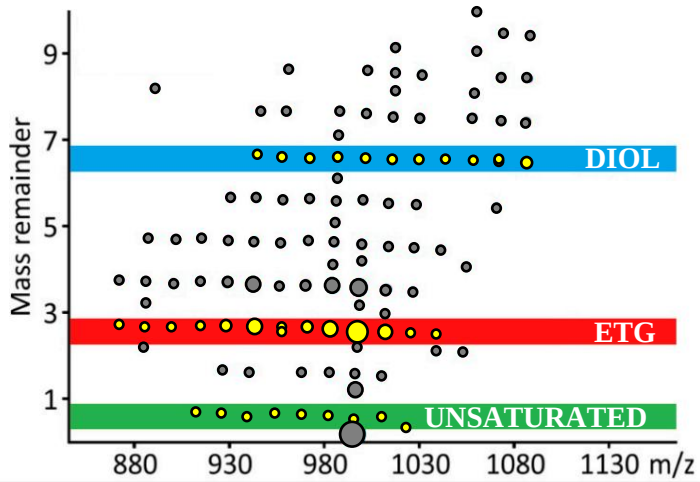

Figure 25 MR *versus* m/z plot of the MALDI-TOF spectrum of the epoxidized soybean oil.

If we zoom the epoxidized triglycerides zone (red highlight), we can easily recognize a number of dots in the corresponding lines then identification the number of epoxide groups and the number of carbon atoms (**Fig. 26**) is possible even visually. Using this figure, the epoxidized triglycerides with no remaining double bonds (if the total (100%) conversion of double bonds to

epoxide groups, DOE = 100%) can be found in the complex mass spectra. All dots on the same horizontal line have the same number of epoxide group. For example, on the third line where there are three epoxide groups indicating the possibility of having three different compositions with various number of carbon atoms. Thus, three dots correspond to the peaks m/z 898, 927 and 955 with the number of carbon atoms of 53, 55 and 57 in the chemical composition of the epoxidized oils, respectively. A difference of 0.0364 in the MR value is due to the replacement of $(CH_2)_2$ moiety by a C_2H_2O (epoxide) group.

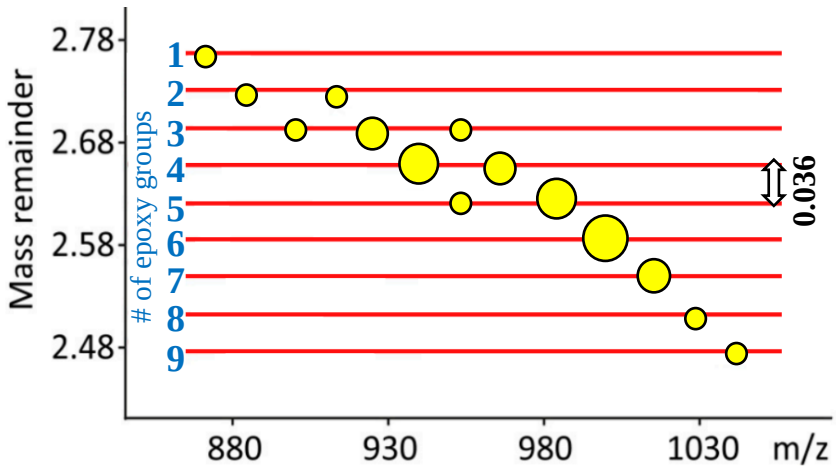

Figure 26 Zoomed MR *versus* m/z plot of the MALDI-TOF spectrum of the epoxidized oils.

Using the following equations, we can calculate the polymer quantities of the epoxidized vegetable oils such as number average molecular weight M_n, the average number (n_n^{NEG}) and average number of epoxide groups weighted by number of epoxide groups (n_w^{NEG}), the polydispersity of the number of epoxide groups (n_n^{NEG}/n_w^{NEG}), average number of carbon atoms (n_n^{C}), and the degree of epoxidation (DOE).

$$M_n = \frac{\sum_{i=1}^{\infty}(I_i \times m_i)}{\sum_{i=1}^{\infty} I_i} \quad (9)$$

$$n_n^{NEG} = \frac{\sum_{i=1}^{\infty}(I_i \times n_i^{NEG})}{\sum_{i=1}^{\infty} I_i} \quad (10)$$

$$n_w^{NEG} = \frac{\sum_{i=1}^{\infty}(I_i \times n_i^{NEG2})}{\sum_{i=1}^{\infty}(I_i \times n_i^{NEG})} \quad (11)$$

$$n_n^{C} = \frac{\sum_{i=1}^{\infty}(I_i \times n_i^{C})}{\sum_{i=1}^{\infty} I_i} \quad (12)$$

where I_i is the intensity of the peak of interest, m_i is the molecular weight of the ETGs, and n_i^{NEG} is the number of epoxide groups in a molecule. **Table 7** summarizes the characteristics of the epoxidized soybean and linseed oils.

Table 7 Characterization of the epoxidized soybean and linseed oils.

	soybean oil	linseed oil
$\mathbf{M_n}$	950	990
$\mathbf{n_n^{NEG}}$	5.12	7.23
$\mathbf{n_w^{NEG}}$	5.45	7.60
$\mathbf{n_n^{NEG}/n_w^{NEG}}$	1.06	1.05
$\mathbf{n_n^{C}}$	56.4	56.8
DOE	99.1	99.1

Although molecular weights of the epoxidized soybean and linseed oils are close to each other, there is a difference in the average number and average number of epoxide groups weighted by the number of epoxide groups. Average number of carbon atoms and the degree of epoxidation of two vegetable oils are similar.

The knowledge of polymer quantities of these epoxidized vegetable oils is very important in designing, planning and production of eco-friendly polymers.

4.2 Investigation of the structure of the epoxidized triglycerides

After determining the chemical compositions of the epoxidized vegetable oils, we get the structural information on the epoxidized triglycerides by applying ESI-QTOF MS/MS. First, samples with different ionization agents such as Na^+, Li^+ and NH_4^+ were measured. **Figures 27**, **28** and **29** show tandem mass spectra of sodium, ammonium and lithium adducts of the soybean oil, respectively.

As seen in **Figures 27**, **28** and **29** the epoxidized triglycerides with different adducts undergo various fragmentation reactions in the collision-induced dissociation process. Fragmentation of the triglycerides with sodium cation is the simplest where the reactions yield only an epoxidized diglyceride and a single epoxidized fatty acid (**Fig. 27**). Here, there are only four different fatty acid losses. On the lower mass range, three peaks of fatty acids (epoxidized oleic acid, epoxidized linoleic acid and epoxidized linolenic acid, from left to right) can be seen.

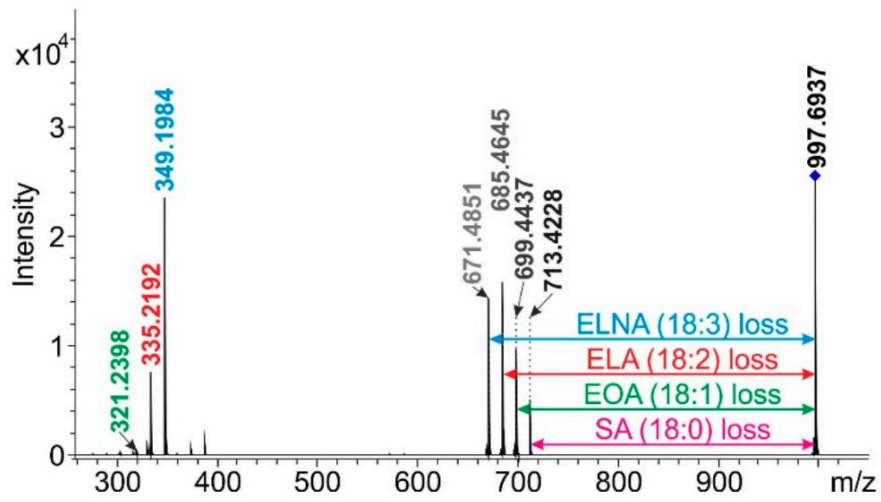

Figure 27 MS/MS spectrum of the sodium ETG adduct at m/z 997 of the soybean oil (70 eV).

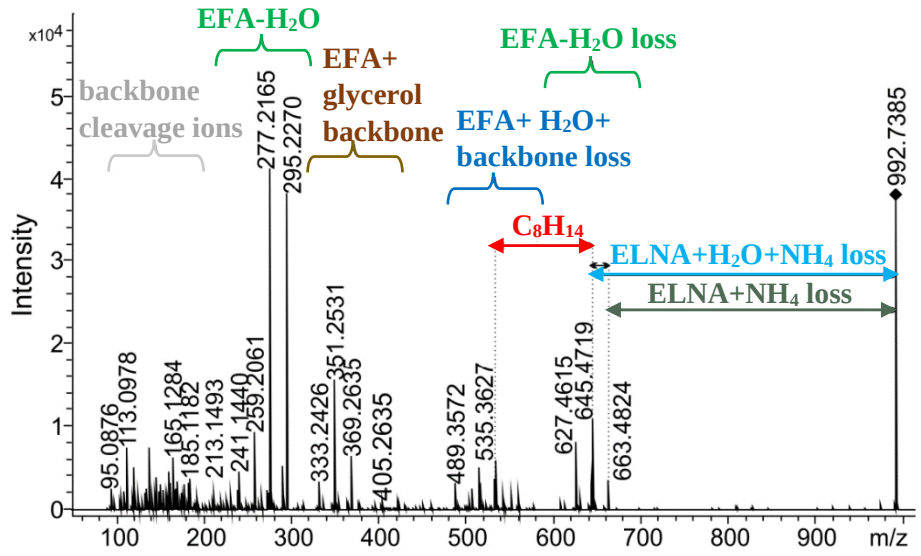

Figure 28 MS/MS spectrum of the ammonium ETG adduct at m/z 992 of the soybean oil (36 eV).

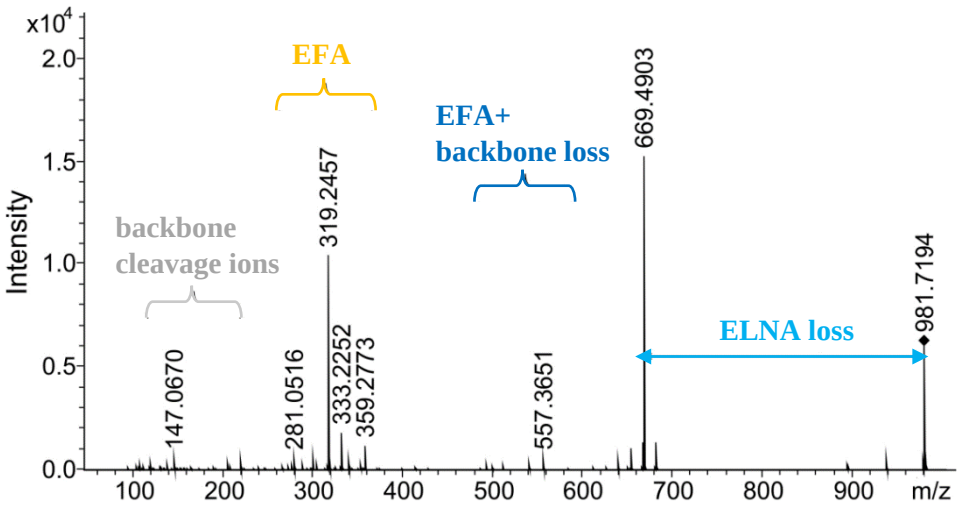

Figure 29 MS/MS spectrum of the lithium ETG adduct at m/z 981 of the soybean oil (65 eV).

Fragmentation of the triglycerides with ammonium cation ($[M+NH_4]^+$) (**Fig. 28**) is very harsh. Besides a huge number of product ions, there are many peaks with lower intensity, which cannot be identified. Backbone cleavage of the ions and epoxidized fatty acid plus glycerol backbone fragments are also observed. Epoxidized fatty acid and water losses can be found in the lower and higher mass range of this spectrum. Epoxidized linolenic acid loss formed in both sodium (**Fig. 27**) and lithium adducts of the (**Fig. 29**) triglyceride fragmentations by tandem mass spectrometry. Backbone cleavage ions are also found in the spectrum of lithium triglyceride adducts. **Table 8** demonstrates the possible structure of product ion of the epoxidized diglycerides and single epoxidized fatty acids along with mass/charge values.

Table 8 Structures of fragment ions of the epoxidized soybean oil with tandem mass spectrometry.

m/z	Structure
335.2192	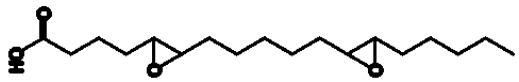
349.1984	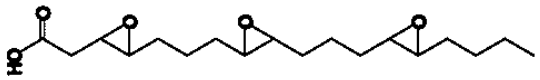
671.4851	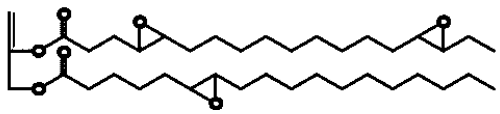
685.464	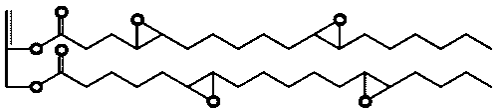

699.4437	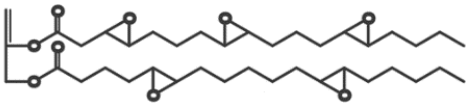
713.4228	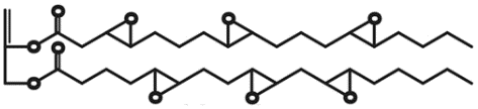

The sodium adduct ion of the epoxidized linseed oil was also measured using tandem mass spectrometry (**Fig. 30**). Here, we can observe similar fragmentation pattern to that of the sodium adducts of epoxidized soybean oil. Thus, epoxidized oleic acid, epoxidized linoleic acid, epoxidized linolenic acid and stearic acid losses were also found in the case of the epoxidized linseed oil.

Although the same precursor ion and collision energy were selected for both soybean and linseed oils, in spite of the fact that the fragmentation patterns were similar, the intensity ratios of the product ions show large differences. This difference comes from the different amount of the linoleic acid (LA) and linolenic acid (LNA) in the vegetable oils (**Fig. 31**). While ELA is dominant in the soybean oil, ELNA is just 10 percent presents in the epoxidized soybean composition. Stearic acid is the lowest amount of fatty acids constituting the vegetable oils. Other fatty acid amounts are similar in epoxidized oils investigated.

Therefore, the simple product ion spectra of the sodium ETG adducts raise a possibility to easily determine the EFA compositions of these oils by tandem mass spectrometry.

Furthermore, we proposed fragmentation pathways for the ammonium and sodium ETG adducts as illustrated in **Figures 32 and 33**.

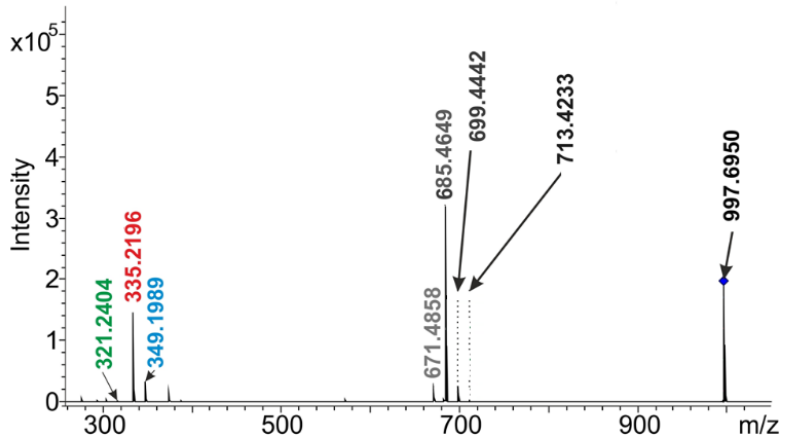

Figure 30 MS/MS spectrum of the sodium ETG adduct at m/z 997 of the linseed oil (70 eV).

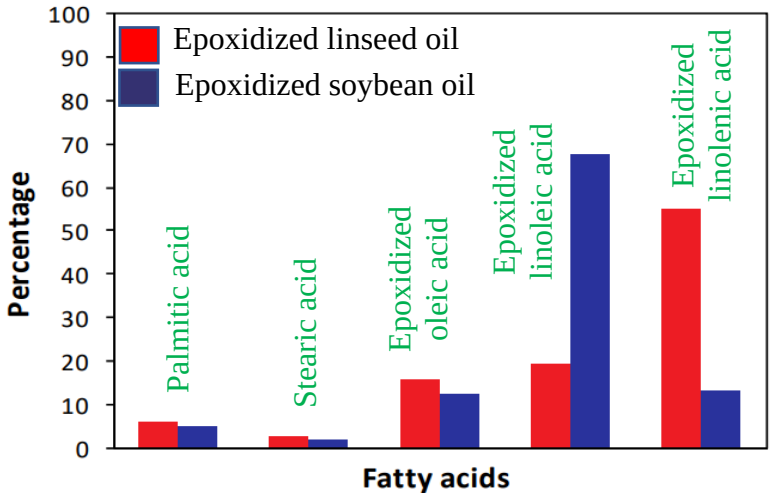

Figure 31 Fatty acid composition of the epoxidized linseed and soybean oils.

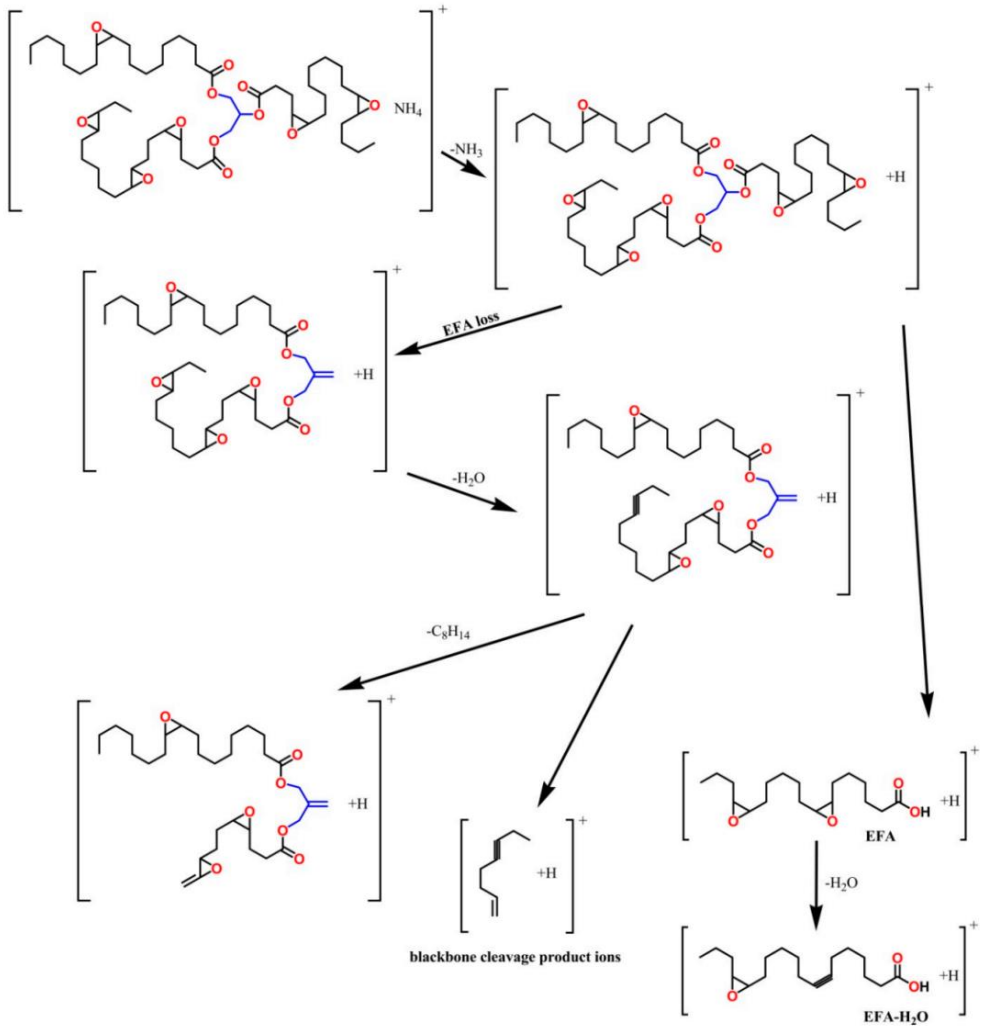

Figure 32 Proposed fragmentation pathways of ammoniated EFA.

As previously discussed about the complexity of the fragmentation of the ammonium adduct of epoxidized triglycerides, we sketched seven possible fragmentation structures (**Figure 32**). Water, EFA, C_8H_{14} losses are common process of caused ammonium adducts of epoxidized triglycerides by CID measurements.

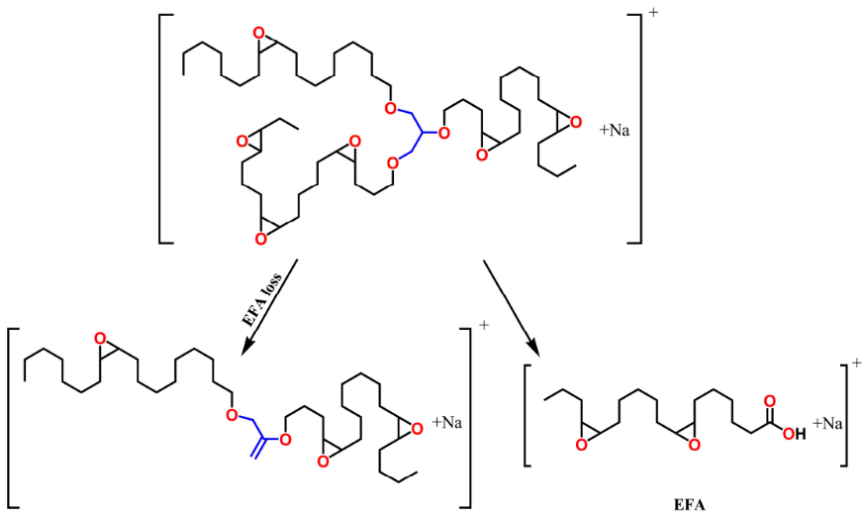

Figure 33 Proposed fragmentation pathways of sodium adduct EFA.

To find the composition of the fatty acids in the epoxidized triglyceride oils, we measured all sodium adduct ETG specimens of each epoxidized soybean and linseed oils at different collision energies in the rage of 40-80 eV. We transformed measured data to the Relative intensity - Collision energy plot. This is called breakdown curve (**Fig. 34 and 35)**. From these figures it is clearly seen that curves of the product ions with two epoxidized fatty acid (EFA) chains decreases above 70 eV and the main fragmentation reaction is the loss of an EFA chain. For example, ELNA lost yields the epoxidized diglyceride and a single epoxidized fatty acid at *m/z* 671 and 349, respectively.

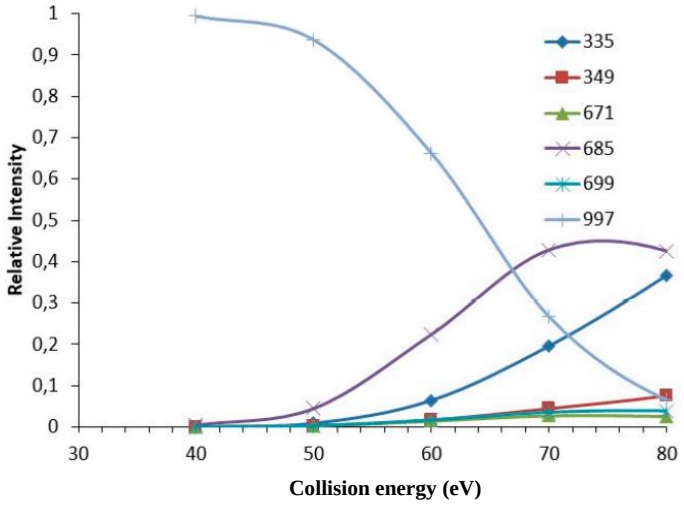

Figure 34 Breakdown diagrams for the fragment ions m/z 335, m/z 349, m/z 671, m/z 685, m/z 399, and the precursor ion m/z 997 of the sodium adduct epoxidized triglyceride (57:6) of the soybean oil.

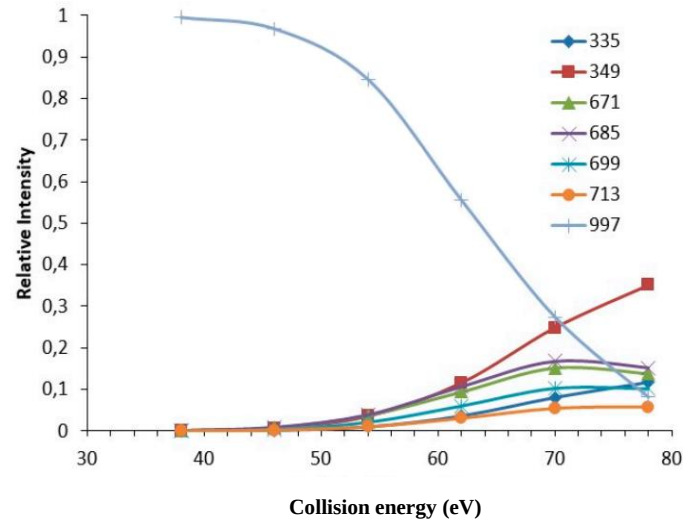

Figure 35 Breakdown diagrams for the fragment ions m/z 335, m/z 349, m/z 671, m/z 685, m/z 399, m/z 713, and the precursor ion m/z 997 of the sodium adduct epoxidized triglyceride (57:6) of the linseed oil.

As the relative intensity of the sum of the product ions at m/z 671 and 349 is related to the sum of all the product ions, the percentage of ELNA in this specimen can be calculated. Performing this calculation for all the specimens and summarizing the percentages of the EFA weighted by the corresponding intensities of the ETG specimens in the MS spectrum provides the percentage of the EFA in the epoxidized triglyceride oil which is shown in **Figure 31**.

4.3 Multistep Mass-Remainder Analysis - Method

Since we introduced mass-remainder analysis method in previous examples, now we will develop and use it as multi-step mass-remainder analysis in polymer blend investigations. As copolymer blends are complex, we should have a sophisticated method to analyse the data obtained from mass spectrometry. In this method, multiple mass remainders are being calculated sequentially. To understand the algorithm of this method, we will explain all the stages step-by-step. As an example, a simple copolymer – PE3500 (**Sample 1**) was selected, and the visualization of this block copolymer will be discussed. PE3500 is an ethylene oxide/propylene oxide (EO/PO) copolymer with approximately 50 m/m % EO content. It was calculated from our measurement recorded by a MALDI-TOF mass spectrometer (**Fig. 36**). In **Figure 36** we can easily identify a peak series with 44 and 58 Da increments, which correspond to the masses of the EO and PO repeat units, respectively.

As a next step using mass-remainder formula Eq (8), discussed in previous chapter, we reveal the homologous series differing only by the number of PO units. After sorting and filtering all the peak, resulted a graph demonstrated in **Figure 37.**

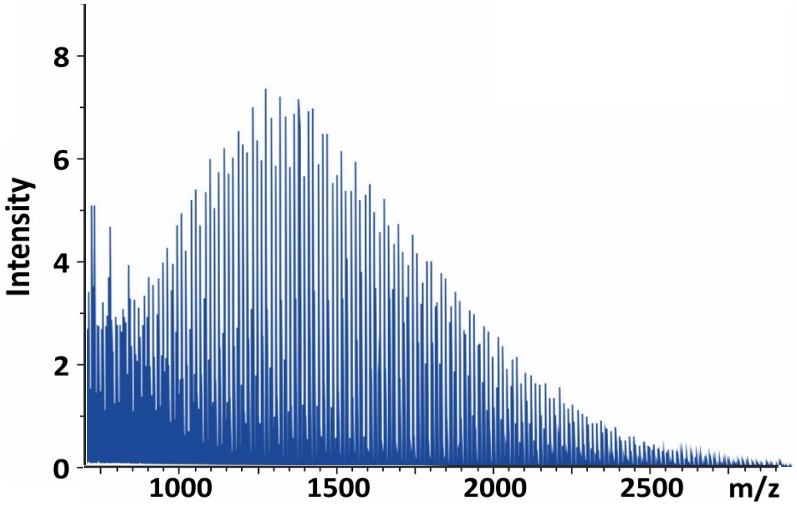

Figure 36 MALDI-TOF mass spectrum of PE3500, Sample 1.

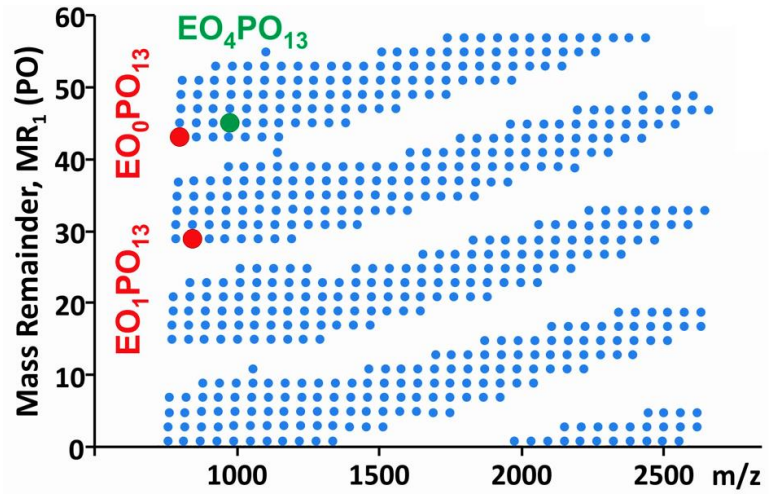

Figure 37 Mass-remainder (MR) *versus m/z* plot of Sample 1.

There are four groups altered vertically to each other by MR_1 = 14.01565, which belongs to the mass difference of the PO and EO repeat units. These shifts come from the addition of one ethylene oxide unit to the copolymer system. For instance, the two selected points in **Figure 37** belong to the compositions EO_0PO_{13} (upper red) and EO_1PO_{13} (lower red). First

remainder is suitable to explore the EO/PO composition of a single copolymer. For complex blend copolymer we should go further to make this plot much "readable". This homologous series can be eliminated to make a plot simpler using the second MARA step Eq (13):

$$MR_2 = MR_1 \; MOD \; R_2 \tag{13}$$

Figures 38 and 39 illustrate MR_2 *versus* m/z plots. The two subseries in **Figure 38** was merged as seen in **Figure 39**. It means that if the difference of R_2 and MR_{2max} (MR_{2max} is the mass of the base unit of the second step - CH2=14.01565) plus MR_2 (**Fig. 38**) equals to n × 1.97927, then MR_2 (**Fig. 39**) will equal to the sum of MR_{2max} and n × 1.97927, where MR_2 and MR_2 are the MR_2 values in **Figures 38** and **39**, MR_{2max} is the MR_2 value of the top line in **Figure 38**, n is a small integer (1, 2, 3, ...) and 1.97927 is the vertical difference between the adjacent lines. After the second step of MARA, each line in **Figure 39** represents a homologous series EO_aPO_b, where a is arbitrary, but the b values are four neighbouring integers. An addition of four EO units to the copolymer results in a shift by 1.97927. This value is the mass difference between oxygen and CH_2 group in the mass remainder *versus* m/z plot, as demonstrated in **Figure 37**: EO_0PO_{13} (upper red) and EO_4PO_{13} (green). This shift belongs to the vertical difference between the adjacent lines in **Figure 38** and **39.**

Comparing the second step to the first step mass remainder analysis plot, many dots on the first-step MR plot was eliminated and ended up with the horizontal "lines" on the second step MR plots. We need another transformation step to eliminate these lines to a single line. Because our aim was to distinguish two different copolymers in polymer blends, thus, the third step was implemented into MARA to accomplish our task.

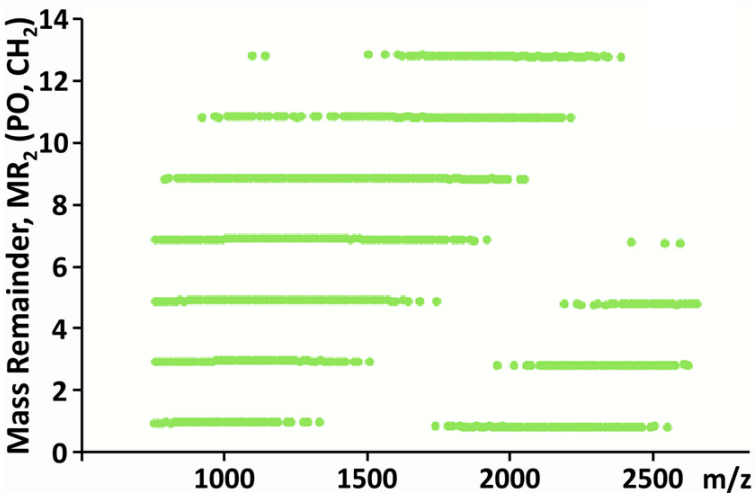

Figure 38 MR_2 *versus* m/z plot of Sample 1.

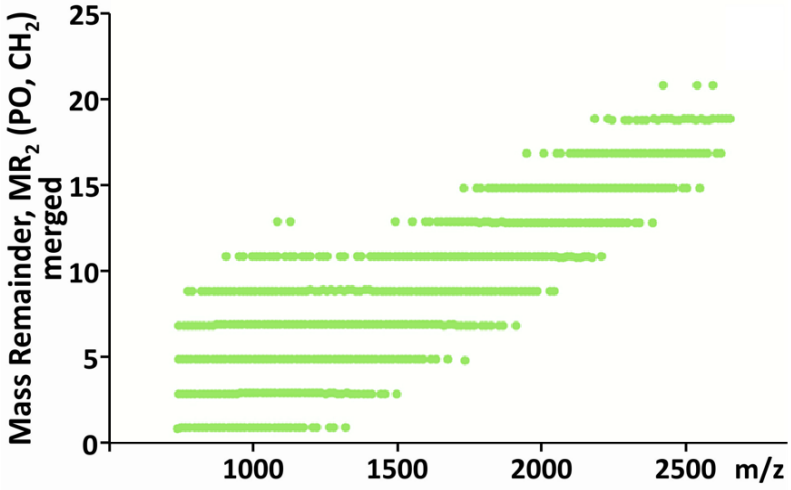

Figure 39 Merged MR_2 *versus* m/z plot of Sample 1.

Going further, performing the third step MARA using Eq (14), the homologous series EO_aPO_b with n values in different vertical groups can be depicted as a single line (**Fig. 40**).

$$MR_3 = MR_2\ MOD\ \ R_3 \tag{14}$$

where R_3 = 1.97927.

The single line in **Figure 40** indicates the presence of only one component in the sample. It is important to note that this component belongs to an EO/PO copolymer chain with the same end group and ionization agent. For example, if we use two copolymers with the same repeat unit but different ionization agents or *vice versa*, two single lines will appear on the third step MARA plot. Because our formula sequentially calculates the remainders, the mass of other ionization cation will cause different value, which directly interferes with the MR values.

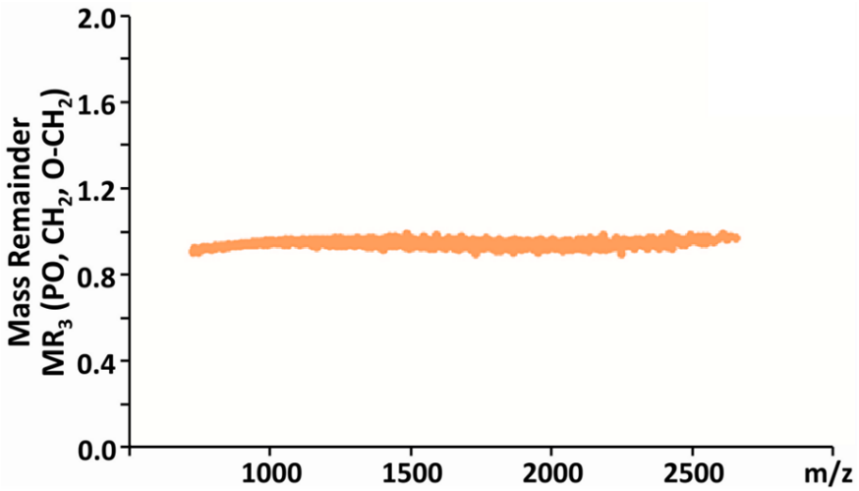

Figure 40 MR_3 *versus* m/z plot of Sample 1.

Additionally, the single line also indicates chemical information, for example the chemical compositions of the compounds which differ by CH_2 and O numbers. If there are other components with different copolymer chain

and even with different ionization agent, additional series would be identified in **Figure 40**. This was a simple example to demonstrate how multi-step MARA works. In the following examples, we will demonstrate the differentiation of various copolymers in polymer blends. Another advantage of our method is the possibility of deisotoping the entire mass spectra. The plots we demonstrated in our studies were already deisotoped. Therefore, a careful selection of the base units needs to have a correct result. Sometimes even−odd filtering of the measured m/z is not easy in the case of the higher molecular weight polymers because of many hydrogen atoms. However, the remainders are determined based on the masses of the monomers including the hydrogen atoms. This is valid if there is no nitrogen atom in the component investigated as it was in the case.

4.4 Differentiation of the composition of polymer blends

4.4.1 Two copolymers with different repeat units in blends

Now we will show polymer blend containing two copolymers with different repeat units. Using multi-step MARA, the visual differentiation of the blends will be possible. PLA/PCL copolymer and the blend with PLA/PCL and PE3100 copolymers were investigated. Base units for both copolymers are different. PE3100 is an ethylene oxide/propylene oxide (C_2H_4O/C_3H_6O) copolymer and $C_3H_4O_2$ is the repeat unit of lactic acid. As previously discussed, the third step of the different masses of the repeat units will result in a separate single line. All measurements are performed with the same ionization agent yielding sodium adducts. **Figure 41** (**a, b**) shows the mass spectra of PLA/PCL copolymer and blend copolymer recorded by a MALDI-TOF mass spectrometer, respectively.

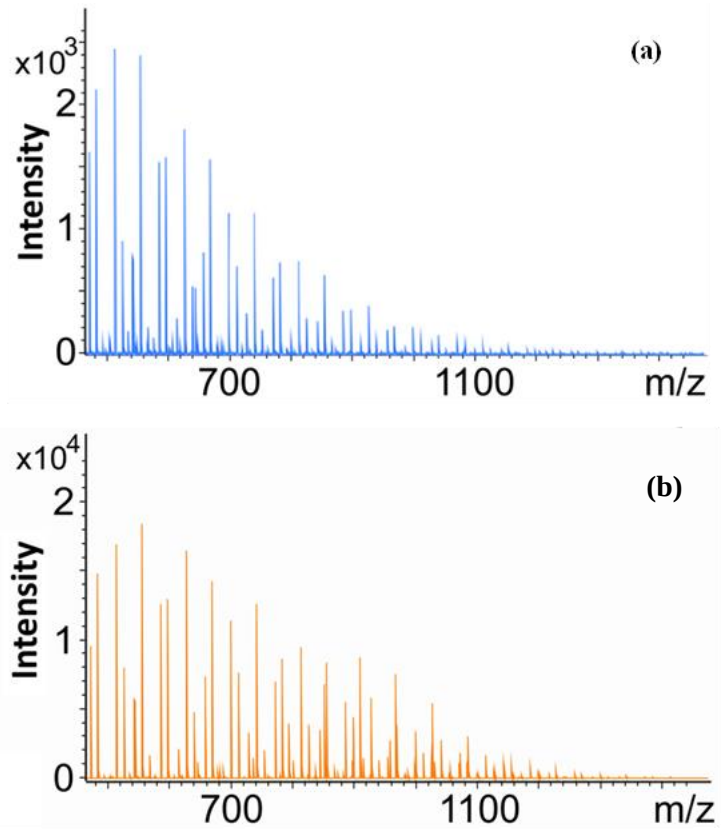

Figure 41 MALDI-TOF mass spectrum of (a) the polylactide/ polycaprolactone (PLA/PCL) copolymer, Sample 2 (b) polymer blend, Sample 3.

Performing the third step MARA, we will be able to identify the composition of the blend easily and quickly. As suitable R_n selection is required by the MARA formulas Eq (8, 13 and 14), we assign the exact mass of the lactic acid repeat unit for R_1 ($C_3H_4O_2$ = 72.02113 Da) as the base unit for the first MARA step. The mass remainder (MR_1) *versus* m/z plots (**Figure 42 a, b**) shows the homologous series differing only by the number of lactic acid repeat units. The characteristic MR difference between the series is 14.01565 (CH_2), which corresponds to one-third of the mass difference between the lactic acid and the caprolactone repeat units. It is possible to determine the composition of the PLA/PCL copolymer in **Figure 42** (**a**).

Therefore, the same figure (**b**) is much more complex with additional small dots of another copolymer. Thus, it is still not enough to differentiate the blend system.

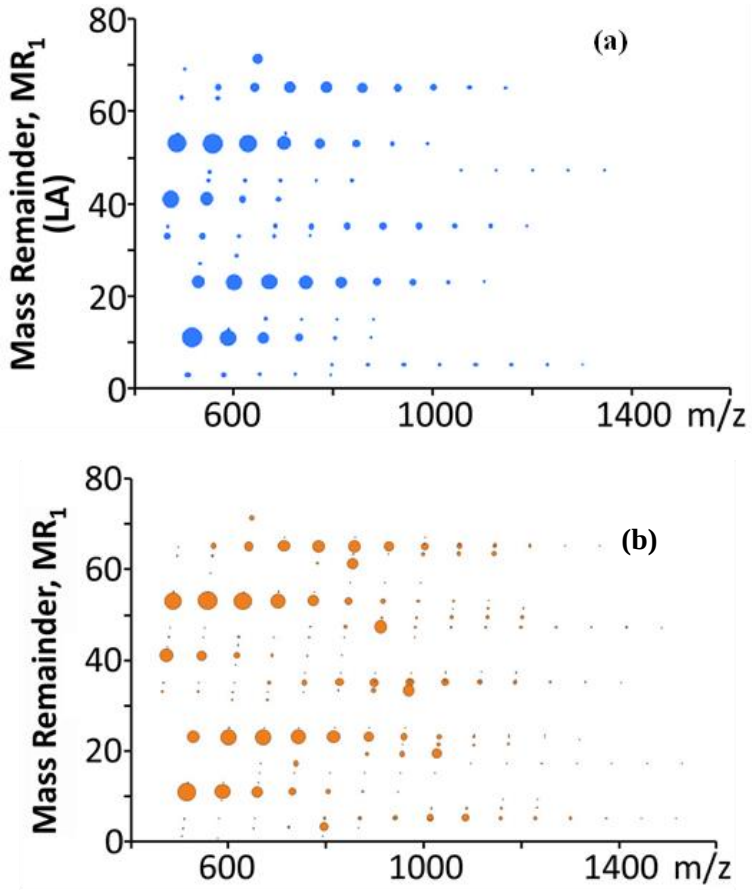

Figure 42 MR_1 *versus* m/z plot of (a) Sample 2 (b) Sample 3.

As in the previous chapter, we should eliminate the number of dots by sorting the same homologous series. Going on the second step MARA, we assign the exact mass of CH_2 for R_2 (14.01565) to make the plot much simpler by decreasing the units in y-axis as shown in **Figure 43**. At a first glance, it is not very easy to determine, which one is a single copolymer or copolymer blend.

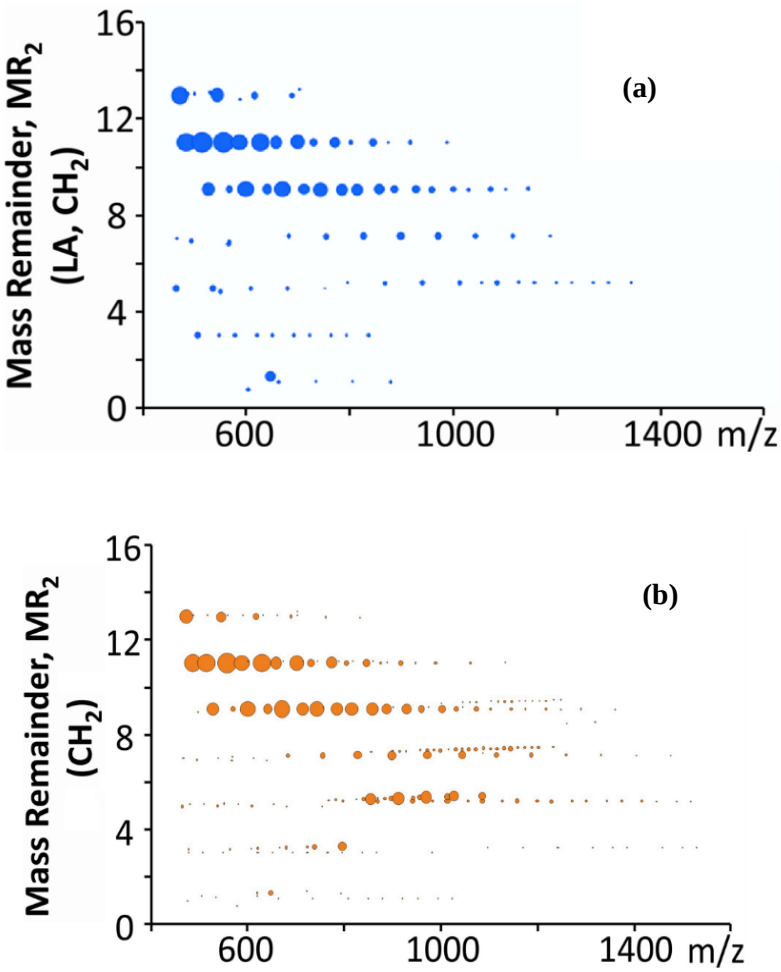

Figure 43 MR_2 *versus* m/z plot of (a) Sample 2 (b) Sample 3.

In the last step, using Eq (14) we process the third step MARA. We assign the exact mass of the difference of oxygen and CH_2 for R_3 (O-CH_2 = 1.97927 Da). This difference comes from y-axis between two adjacent lines in **Figure 43**. After plotting MR_3 vs m/z plot, we can see a single line in **Figure 44** (**a**) where there is only PLA/PCL copolymer. From previous example, we already know that this single line demonstrates only one type of copolymer in the sample. While having a look at **Figure 44** (**b**) we can see another line above PLA/PCL line, which is circled in red. 58 Da as a mass

difference between the adjacent peaks suggests the PO repeat unit. Additionally, three characteristic m/z values - 855.575, 913.623, and 971.654 in this extra series belong to EO_4PO_{11}, EO_4PO_{12}, and EO_4PO_{13}, respectively. So, applying M-MARA method we easily recognized the presence of an addition series in polymer blend. If there is any possible contamination in polymer blend samples, it can be displayed on these plots.

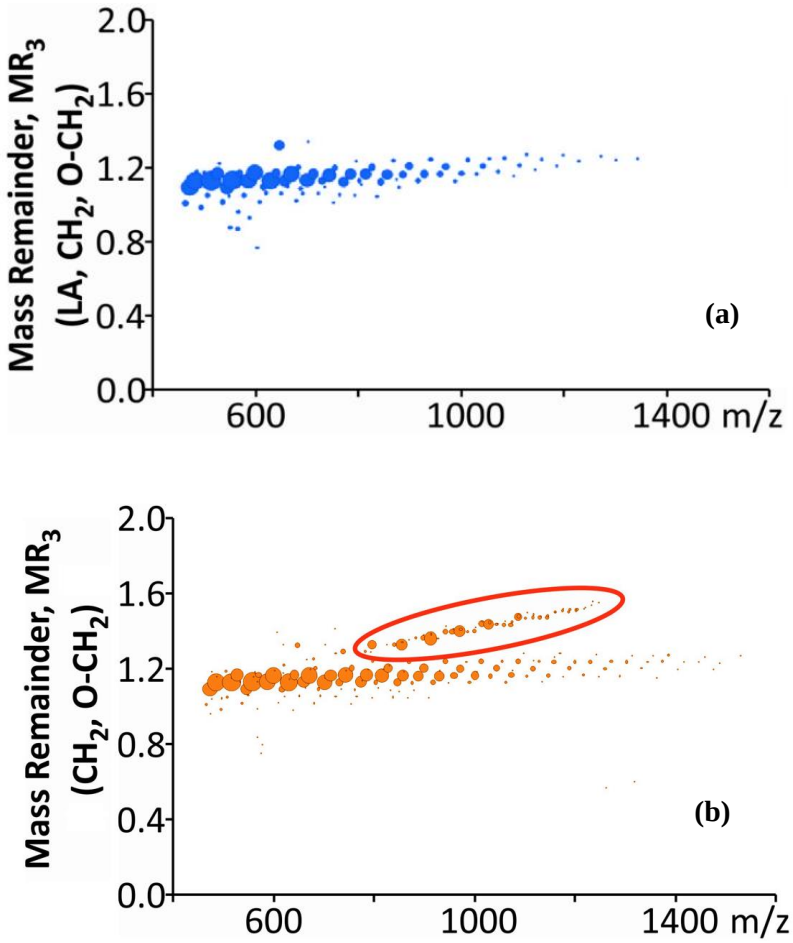

Figure 44 MR_3 *versus* m/z plot of (a) Sample 2 (b) Sample 3.

4.4.2 Two copolymers with the same repeat units in blends

In this section, we differentiated the blends composed of different based polyether polyols: sorbitol and propylene glycol-initiated copolymers, which are six-arm and linear copolymers, respectively. The repeat units in both copolymers are EO/PO type. **Figure 45** illustrates the mass spectrum of the blend containing of two copolymers where the differences between peak series are 44 and 58 Da corresponding to the mass of. EO and PO, respectively. However, knowing only this information it is not enough to compare the peak series and to identify the composition of this polymer blend.

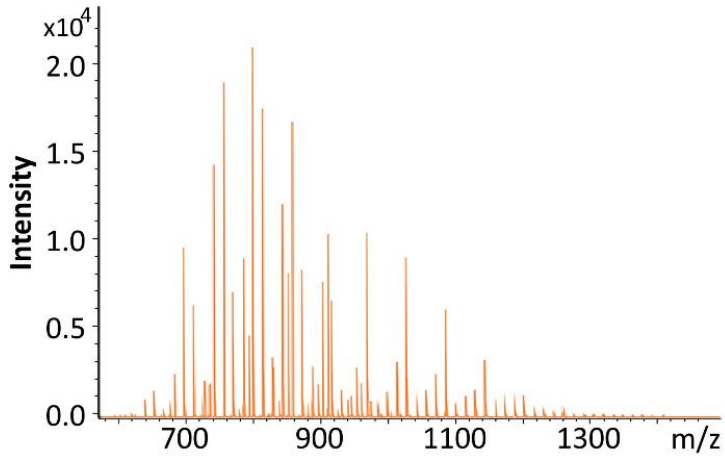

Figure 45 MALDI-TOF mass spectrum of the EO/PO copolymer blend, Sample 4.

The previously calculated MR_3 *versus* m/z plots in **Figure 40** suggested a single line - EO/PO copolymer with the same end group and ionization agent. Repeating these calculations and applying this method for this blend resulted in a single line as shown in **Fig. 46**. Thus, third step MARA did not help to differentiate these copolymers in blends, because both copolymers are hydroxyl terminated and composed of the same repeating EO/PO monomers. They only differ in type of base units. PE3100 is linear

while RF551 is sorbitol-based copolymer. So, it is not possible to differ the copolymers whose base types are different, while the repeat unit are the same using third step MARA.

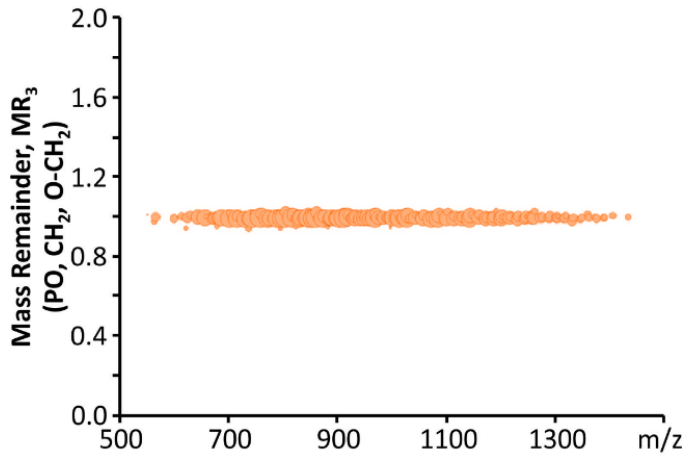

Figure 46 MR_3 *versus* m/z plot of Sample 4.

We take another approach plotting MR_2 *versus* MR_1 where R_1 = 58.04187 and R_2 = 1.97927. To compare the resulted graphs, we plotted **Figures 47** and **48** for Sample 1 (single EO/ PO copolymer) and Sample 4 (EO/PO copolymer blend), respectively. Since both PE3100 and PE3500 copolymers are linear EO/PO type and the average molecular weights are similar. Comparing a single copolymer with a blend copolymer system based on the intensity distribution and discussing the change and shift in the number of ethylene oxide numbers on these plots is favourable.

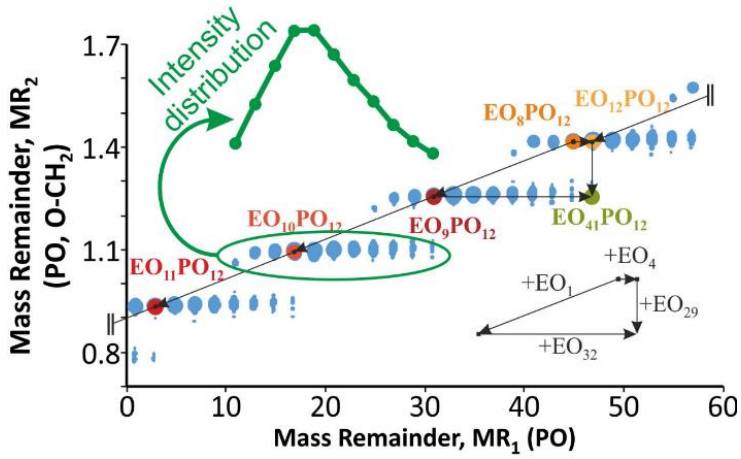

Figure 47 MR_2 *versus* MR_1 plot of Sample 1.

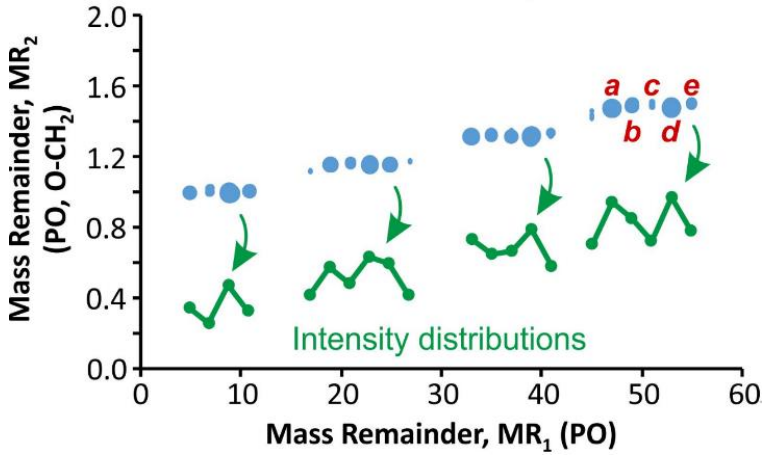

Figure 48 MR_2 *versus* MR_1 plot of Sample 4.

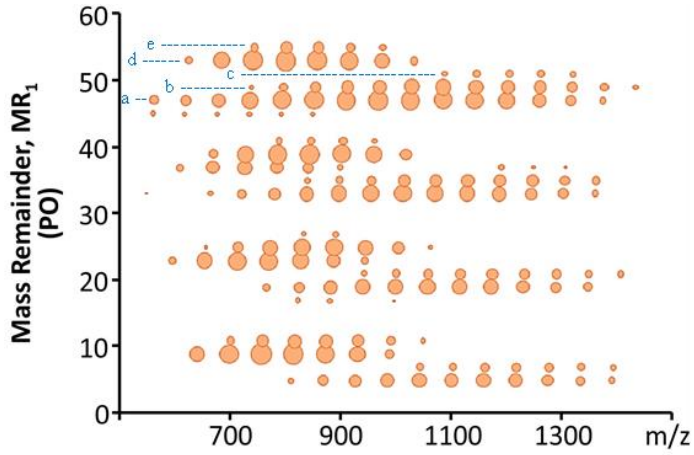

Figure 49 MR_1 *versus* m/z plot of Sample 4.

Figure 49 demonstrates MR_1 *versus* m/z plot of sorbitol and propylene glycol-initiated copolymer blend - Sample 4. Labels a, b, c, d, and e, each dot in **Figure 48** indicates the horizontal rows in **Figure 49**. The number of EO units in the polymer determines the location of each dot in the MR_2 *versus* MR_1 plots (**Figures 47 and 48)**. A single dot has the same number of EO units with any number of PO units. The black arrows at the bottom in **Figure 47** describes how EO change in x and y axis while having the same number of propylene oxide. For example, the neighbouring dots in a row depict EO/PO series differing in four EO units (EO_8PO_{12} and $EO_{12}PO_{12}$) in **Figure 47**. Other differences can be observed on this plot such as an increase by 32 in the number of EO with the same number of PO number along x-axis as well as an increase by 29 in the number of EO with the number of PO along y-axis.

If we add the peak intensity modality concept to our case, it will give us a significant hint to differentiate the complex blend systems. Both **Figures 47** and **48** were plotted based on their intensity distribution of the number of EO units. For example, the intensity distribution of the peak series circled in

green in **Figure 47** shows unimodal distribution. As it can be seen from the size of the dots. Therefore, the intensity distribution (indicated by green points) of the rows in **Figure 48** reveals bimodal distributions. So, based on the complexity of the intensity modality we differentiate the sample whether it is a single copolymer or a copolymer blend. Thus, unimodal and bimodal distribution correspond to a single copolymer and a copolymer blend, respectively.

In contrast to previous copolymer blend, now we blend the same type of high molecular weight copolymers consisting of EO/PO monomers. **Figures 50** and **51** show the mass spectra of Sample 5 (a single $EO_x{-}PO_y{-}EO_x$ copolymer) and Sample 6 (blend of it with a $PO_x{-}EO_y{-}PO_x$ copolymer), respectively. Because of high molecular weight of both copolymers, spectra become more complex due to the presence of many peaks making impossible to determine whether they are single copolymers or blends. As these copolymers have the same repeat units and end groups, the third step MARA will not be advantageous to differentiate the blend systems.

In this case, we make the intensity scaled MR_2 *versus* MR_1 plots to evaluate the composition of the samples. **Figures 52** and **53** show the plots of Samples 5 and 6, respectively. The same R_1 and R_2 values were selected as in previous calculation. The size of the dots in each group determines the distribution of the number of EO units. Sample 5 (**Fig. 52**) where there is only a single copolymer showing unimodal distribution while Sample 6 is copolymer blend (**Fig. 53**), having bimodal intensity distribution.

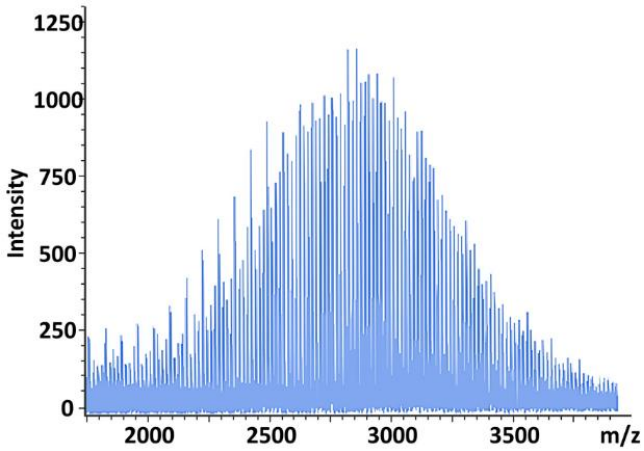

Figure 50 MALDI-TOF mass spectrum of the EO/PO copolymer, Sample 5.

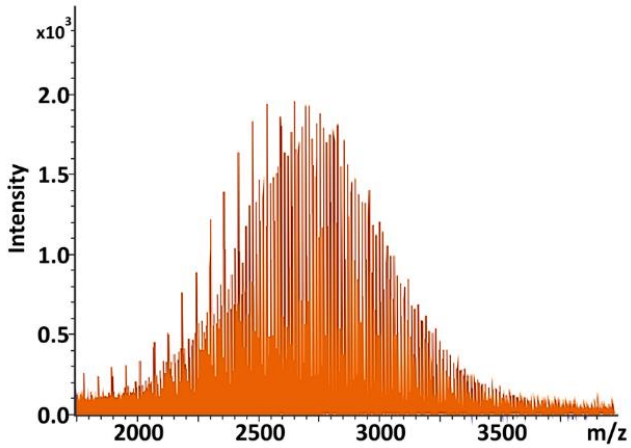

Figure 51 MALDI-TOF mass spectrum of the EO/PO copolymer blend, Sample 6.

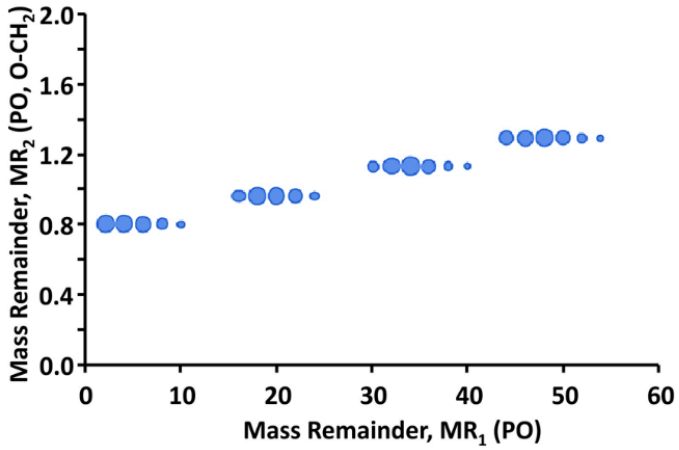

Figure 52 MR_2 *versus* MR_1 plot of Sample 5.

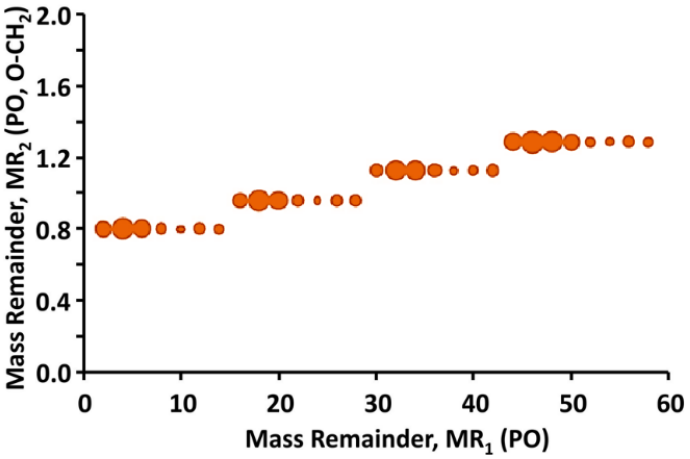

Figure 53 MR_2 *versus* MR_1 plot of Sample 6.

We also checked the KMD plot for the blend copolymer (Sample 6). As seen in **Figure 54**, there are two groups of dots, which show the presence of different copolymers and easily distinguishable two components in the sample. The disadvantage of this method is that determination of the monomers is not possible because of the lack of effective filtering of data.

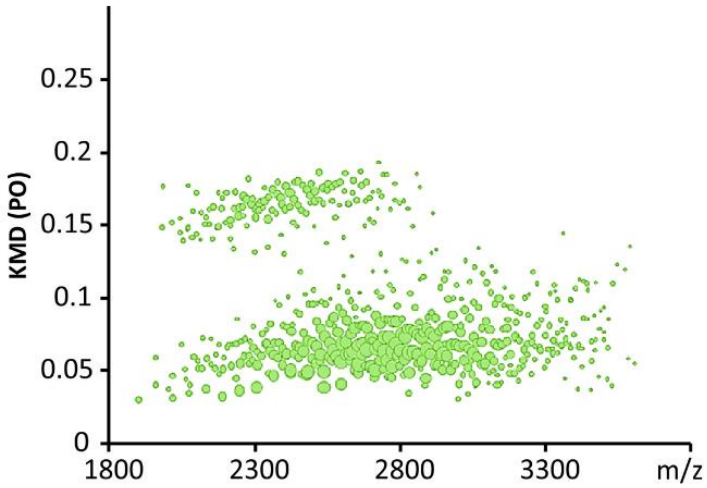

Figure 54 KMD plot of Sample 6.

4.5 Tandem Mass-Remainder Analysis of polyether polyols

In the previous examples we studied different samples and characterization/differentiation of complex systems applying MARA method. In this section we will go further and investigate tandem mass spectrometric characteristics of various types of polyether polyols. To get simplified graphical representation of the MS/MS spectra, we developed and applied Multistep Mass-remainder analysis method (M-MARA).

The mass spectrometric analysis of different based polyether polyols such as glycerol, sorbitol is very difficult because of overlapping peaks as well as isobar and isomer compounds. **Table 9** demonstrates some isomer/isobar molecular species for polyether polyols.

Table 9 List of isomer/isobar molecular species of polyether polyols.

Type	Structure	Elemental Composition	Monoisotopic Mass (Da)
diol	$H_2O(C_2H_4O)_9(C_3H_6O)_3$	$C_{27}H_{56}O_{13}$	588.3721
triol	$C_3H_8O_3(C_2H_4O)_6(C_3H_6O)_4$	$C_{27}H_{56}O_{13}$	588.3721
tetraol	$C_5H_{12}O_4(C_2H_4O)_5(C_3H_6O)_4$	$C_{27}H_{56}O_{13}$	588.3721
hexaol	$C_6H_{14}O_6(C_2H_4O)_0(C_3H_6O)_7$	$C_{27}H_{56}O_{13}$	588.3721
tetraol	$(NH_2)_2C_2H_4(C_2H_4O)_{12}(C_3H_6O)_0$	$C_{26}H_{56}N_2O_{12}$	588.3833

As it turns out from **Table 9**, different types of isomeric copolymers such as diol, triol, tetraol and hexaol have the same mass depending on the replacement of the EO and PO numbers and also the type of initiator. With the same mass unit of 588.3721 Da ($C_{27}H_{56}O_{13}$) these four copolymers cannot be differentiated. Also, nitrogen containing tetraol type polyether polyol is isobar compound with the mass of 588.3833 Da. In this case, using normal mass spectrometric measurements we will not be able to differentiate the polyether polyols listed in **Table 6**. To describe and discuss the method both single mass and tandem mass spectrometric measurements were performed of these polyether polyols with ESI-QTOF instrument.

Figure 55 shows the ESI-MS spectra of various types of polyether polyols dominated by the lithium-attachment ions where (a), (b), (d) and (e) are linear polyethylene glycol, linear polypropylene glycol, glycerol base propylene glycol and sorbitol base polypropylene glycol homopolymers, respectively. (c) and (e) are linear polyethylene/polypropylene glycol and sorbitol base polyethylene/polypropylene glycol copolymers.

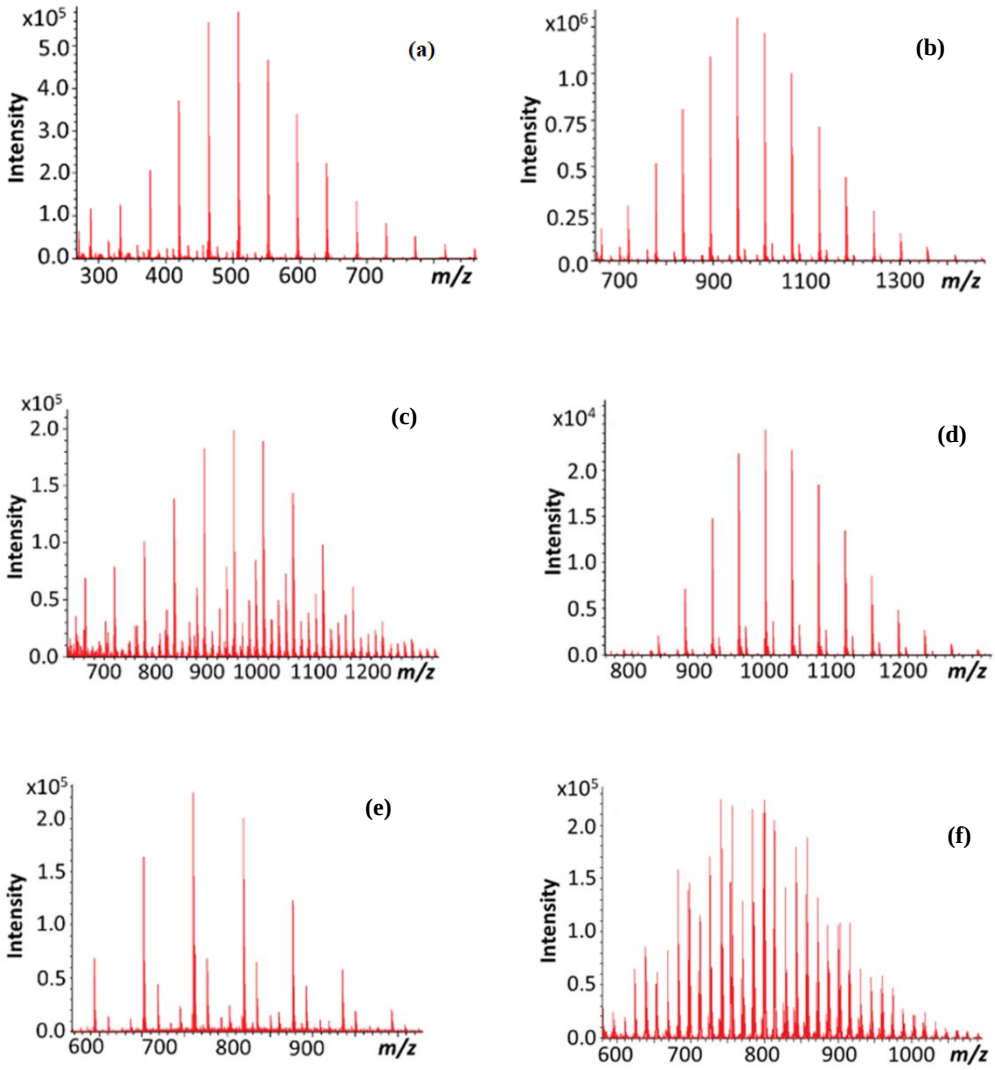

Figure 55 ESI-MS spectra of the polyether polyols (a) PEG (diol), Sample 10 (b) PPG (diol), Sample 11 (c) PEG/PPG copolymer (diol), Sample 12 (d) PPG (triol), Sample 13 (e) PPG (hexaol), Sample 14 (f) PEG/PPG (hexaol), Sample 15.

Some spectra in **Figure 55** displays additional peak series with lower intensity which are different cations.

As discussed in previous sections, applying multi-step MARA, Eq (15) performs the sequential calculations of remainders that eliminates homologous series present in mass spectrum.

$$MR_3 = [(m/z\ MOD\ R_1)\ MOD\ R_2]\ MOD\ R_3 \quad (15)$$

where MOD Excel operation finds the mass remainders after the division by R_n.

R_n values were chosen as 58.04187, 1.979265 and 0.160795 for R_1, R_2 and R_3, respectively. Because all polyether polyols including glycerol and sorbitol base contain only EO and PO repat units. To eliminate the periodicity, we took PO, 4×EO-3×PO, and 22 × PO-29 × EO as MARA base units. Following this rule, we plotted MR_3 *versus* m/z graph for the polyether polyols demonstrated in **Figure 56**.

As seen in **Fig**. **56**, EO/PO replacements were eliminated and yielded single lines. It is important to note that here different single lines do not indicates the presence of other components in the sample. We already discussed in previous chapters that on MR_3 *versus* m/z plots in the case of presence of another ionization agents, because of different m/z, it directly affects to calculate mass remainders. That is why we see different line series on the third mass remainder plots. Since these plots are based on single mass spectrometric measurements, we expect different series only in tandem mass because of fragmentation induced by collision-induced dissociation (CID) in the collision cell of the ESI-QqTOF MS.

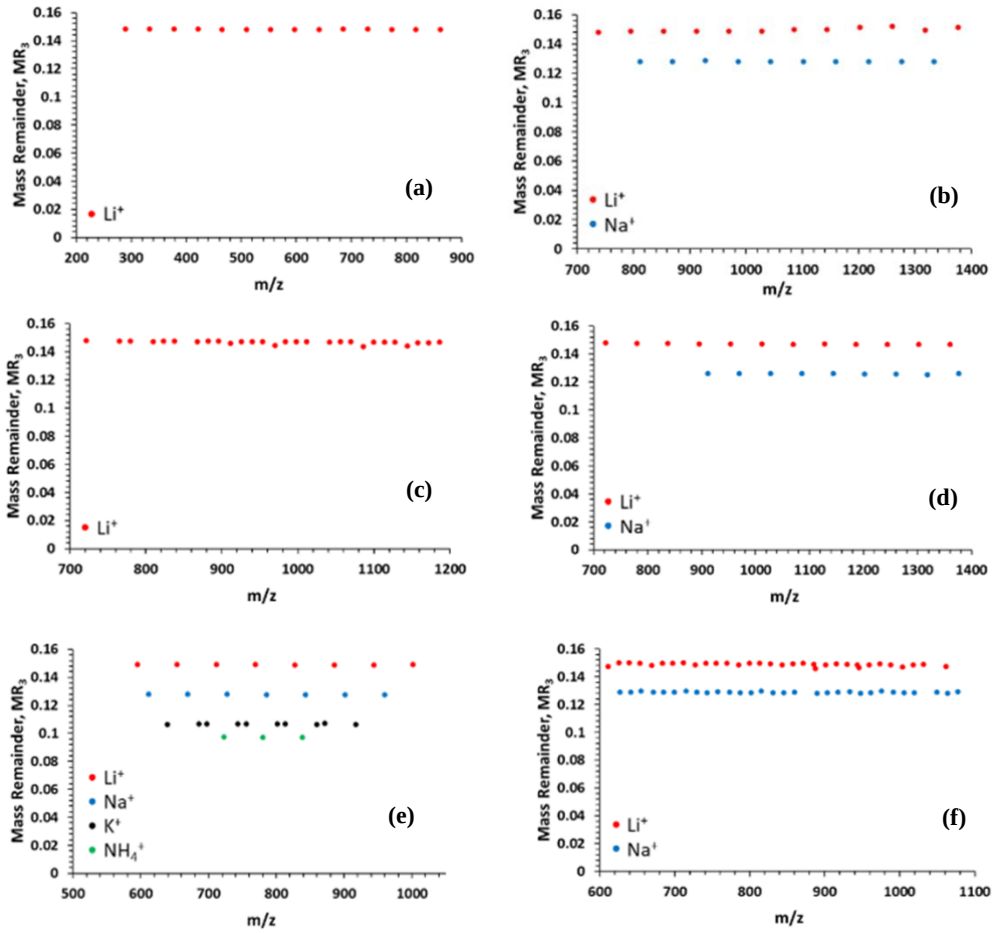

Figure 56 MR_3 *versus* m/z plots of (a) Sample 10 (b) Sample 11 (c) Sample 12 (d) Sample 13 (e) Sample 14 (f) Sample 15.

As seen in **Figure 56**, in addition to the commonly observed lithium protonated molecules, sodium, potassium, and ammonium adducts are also observed. These protonated adducts become feasible as the surface excess charge of ESI nanodroplets may be carried by different cationic components.

Among these, protons are by far most common; nevertheless, sodium, ammonium, and potassium cations cannot be neglected or removed from the system.

These ions come from the mobile phase additives, solvent impurities, glassware, and so on. Therefore, our scope is to investigate all polyether polyol spectra with lithium cation. Additionally, the target lithium-attached ions can be filtered easily by its specific MR_3 value in M-MARA plot as shown in **Figure 57**.

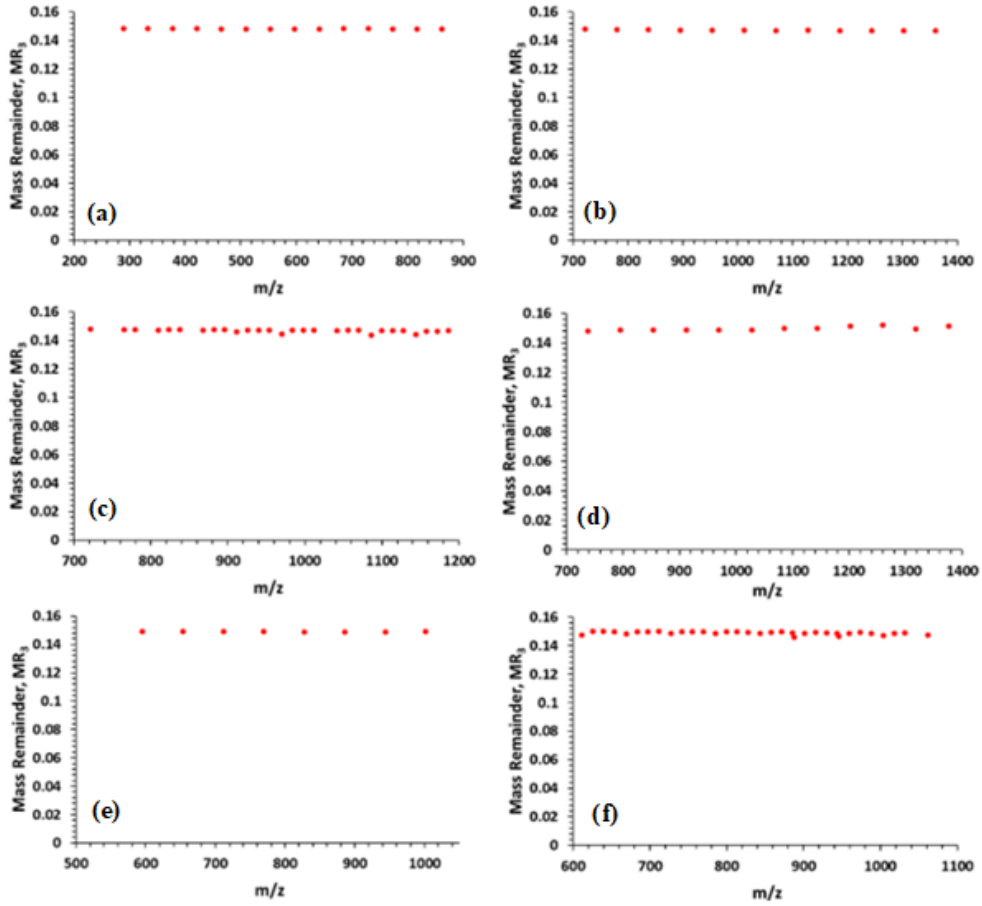

Figure 57 MR_3 *versus* m/z plots (with Li-attached ions) of (a) Sample 10 (b) Sample 11 (c) Sample 12 (d) Sample 13 (e) Sample 14 (f) Sample 15.

After filtering, the MARA plots show only a single horizontal line with lithium-attached ions at MR_3 = 0.149 for all linear, glycerol-, and sorbitol-based polyether polyols. All six homo/copolymers are EO/PO type with different initiators. M-MARA eliminated all the homologue series with the same pattern. That is why only a single line was observed.

To select appropriate R base units for each step of MARA method is very important. The aim of MARA is to simplify the complex data in the plots and make it easy to visualize. For example, in polymer blend investigation R numbers were selected as PO, CH_2 and O-CH_2. This selection depends on the target of the work. But the aim is the same for all MARA methods to simplify and to produce straightforward plots.

For tandem mass spectra our aim was to get efficient sorting by selecting suitable R values. In this section, we selected R_1 for PO value as we did in polymer blends. Mass remainder series are created, and the chemical composition of the components can be defined based on MR_1 *versus* m/z plot. Therefore, generating series for complex systems specially for tandem mass spectra is fuzzy. The second and third step of MARA can be determined from the series of the first mass remainder values. If adjacent MR_1 values are not the same, the difference between mass remainders can be chosen as the base unit for the next steps of MARA. For instance, in our case of EO/PO copolymer systems, the MR_1 *versus* m/z plot composed of multiple series of MR-lines in x axis with typical differences among them. These differences are arising from the replacement of EO/PO units, as 14.015650, 1.979265 and 0.160798 regarding to the replacements of PO-EO, 4EO-3PO and 22PO-29EO, respectively. We expect the similar differences for the series in the tandem mass spectrum of these polyols. Lasty, the third step of MARA displayed a single line by eliminating the periodicities generated by the EO/PO replacements. Therefore, because of different structures of various based

polyether polyols, fragmentation yields other peaks that differs from each other revealed by MS/MS as seen in **Figure 58**.

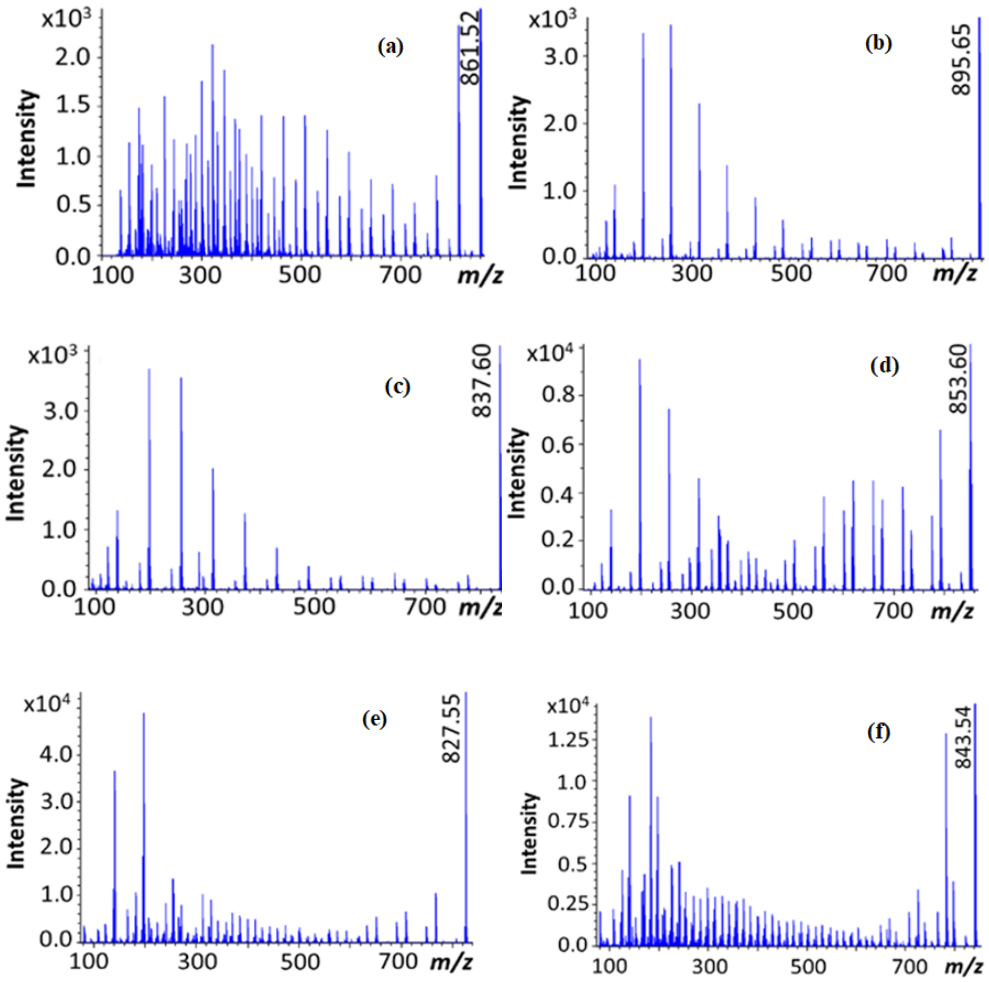

Figure 58 ESI-MS/MS spectra (with Li-attached ions) of (a) Sample 10 (b) Sample 11 (c) Sample 12 (d) Sample 13 (e) Sample 14 (f) Sample 15.

As seen in **Figure 58**, tandem spectra of polyether polyols, especially copolymers seem to be complex and manual assignment of each peak is time consuming. For example, although Sample 10, Sample 13 and Sample 14 are linear EO type, glycerol base PO type and sorbitol base PO type homopolymers, respectively, their MS/MS spectra yielded much more complex peaks similarly to in sorbitol base EO/PO type copolymer, Sample 15. Or *vice versa*, the spectrum of the linear EO/PO type copolymer, Sample 12, yielded very simple product ions. Thus, generated spectrum is characteristic and does not depend on whether it is a homopolymer or a copolymer. Now using the same method and formula Eq (15), we will simplify the complex spectra and differentiate the structural differences between the diol, triol and hexaol polyether polyols. **Figure 59** shows the MR_3 *versus* m/z plots of the MS/MS spectra of different types of polyether polyols.

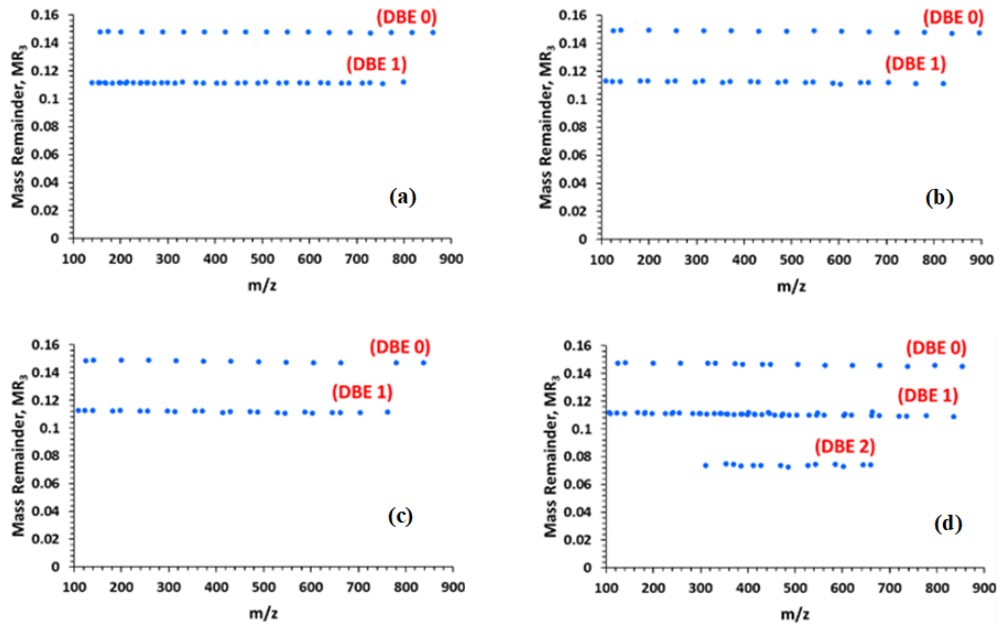

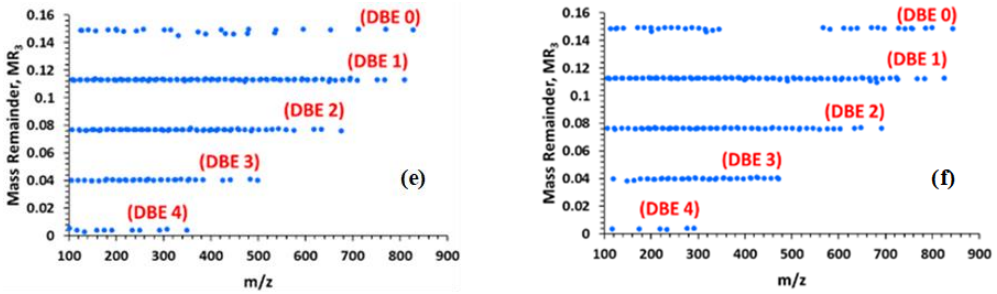

Figure 59 MR_3 *versus* m/z plots of the MS/MS spectra (with Li-attached ions) of (a) Sample 10 (b) Sample 11 (c) Sample 12 (d) Sample 13 (e) Sample 14 (f) Sample 15.

As seen in **Figure 59**, EO/PO copolymers, the different MR-lines have different DBE (double bond equivalent) values. The number of DBE increases as the number of arms of polyether polyol increases. There is maximum 1, 2 and 4 DBE values of diol, glycerol- and sorbitol-based polyether polyols, respectively.

Based on the fragmentation patterns of polyols, we proposed product ion series of the diol type copolymers. **Table 10** shows the possible product compositions with their MR_3 values.

Table 10 Product ion series of diol type polyether polyol copolymers.

Series	Formula	Chain termination	MR_3
A	$Li[HO(C_2H_4O)_n(C_3H_6O)_mH]^+$	- H	0.149
B	$Li[HO(C_2H_4O)_n(C_3H_6O)_mCHCH_2]^+$	vinyl	0.113
B	$Li[HO(C_2H_4O)_n(C_3H_6O)_mCHCHCH_3]^+$	vinyl	0.113
C	$Li[HO(C_2H_4O)_n(C_3H_6O)_mCH_2CHO]^+$	formyl	0.113
C	$Li[HO(C_2H_4O)_n(C_3H_6O)_mCHCH_3CHO]^+$	formyl	0.113
	H_2		0.036

A product ion series corresponds to MR_3 = 0.149, where the ions were formed by losses of monomeric (EO or PO) units. The **B** and **C** fragments are generated by H_2 elimination resulting DBE = 1. The additional rows in the MR_3 vs m/z plots of the three-arm and six-arm polyethers are related to DBE = n, at MR_3 = 0.149 -n × 0.036, where n = 2, 3, 4. We can come to the conclusion that bonds between the arms and the glycerine or sorbitol base are rather weak compared to the bonds in the linear diol polyethers, therefore, multiple collisions between the fragment ions and the collision gas result in further decomposition. Thus, DBE values of the polyether polyols were produced depending on the type of the base and they are independent of being homopolymer or copolymer. For example, both linear homopolymer, Sample 10 and linear copolymer, Sample 3, produced the maximum number of DBE value of 2, which is also sorbitol base homopolymer, Sample 14 and sorbitol base copolymer, Sample 15 generated the maximum number of DBE value of 5.

4.6 Collision-induced dissociation (CID) analysis of the polyether polyols

After tandem mass spectrometric characterization of different polyether polyols, survival yields (SY) of these polymers at different collision energies were studied. SY is a quantitative measure to quantify the efficiency of fragmentation of the precursor ions. It is calculated as the ratio of the precursor ion intensity to the sum of all fragment ion plus precursor ion intensities. In this section we will show the molecular mass dependence of $CCV^{20\%}$ (**Fig**. **60**) for polyols where $CCV^{20\%}$ means characteristic collision voltage at the value of survival yield of 0.2.

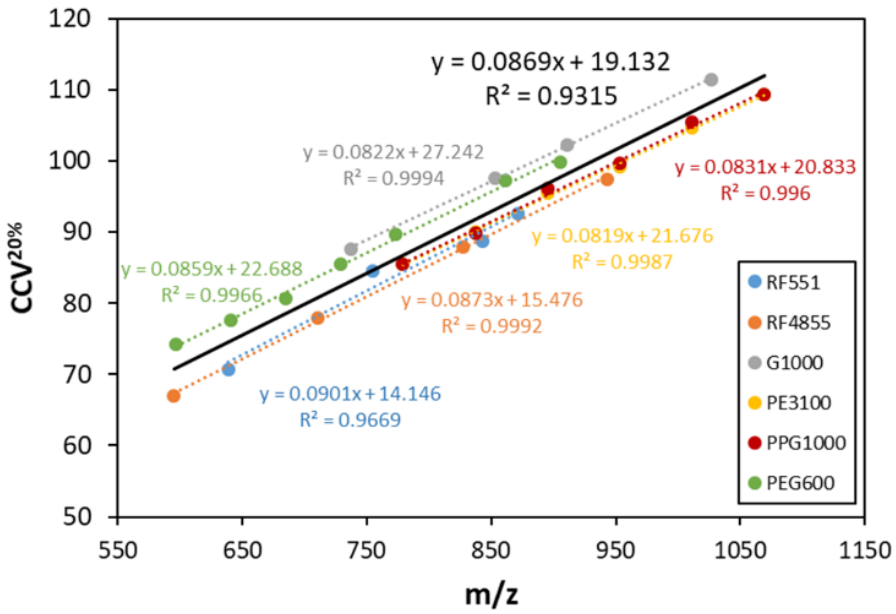

Figure 60 $CCV^{20\%}$ vs m/z plots of the polyether polyols.

As it can be seen in **Figure 60**, linear relationship was obtained between the $CCV^{20\%}$ values and the mass-to-charge ratio for six polyether polyols. All lines are parallel and close to each other. This finding suggests an easy method to adjust the collision energy to get structural information, especially to compare the polyether polyols based on the DBE values in M-MARA plots. The collision energy/voltage can be quickly calculated according to the selected precursor ion mass for the MS/MS analysis by taking an approximate average value of the $CCV^{20\%}$ *versus* m/z as a calibration curve (**Fig**. **60**, black line). Setting the collision voltage to "$CCV^{20\%}$ *versus* m/z calibration", the DBE values precisely differentiate the various types of polyether polyols

Furthermore, molecular mass dependence of $CCV^{50\%}$ (**Fig. 61**) where the collision voltage necessary to obtain 50% fragmentation was also studied. In this percentage the intensity of precursor ion equals to the sum of fragments ion. This is a traditional method to study characterization of different compounds. So, this is interesting to see the differences and select the best collision energy to investigate the characterization. Here, all polyether polyols also show the same pattern, i.e., linear correlation and lines parallel to each other.

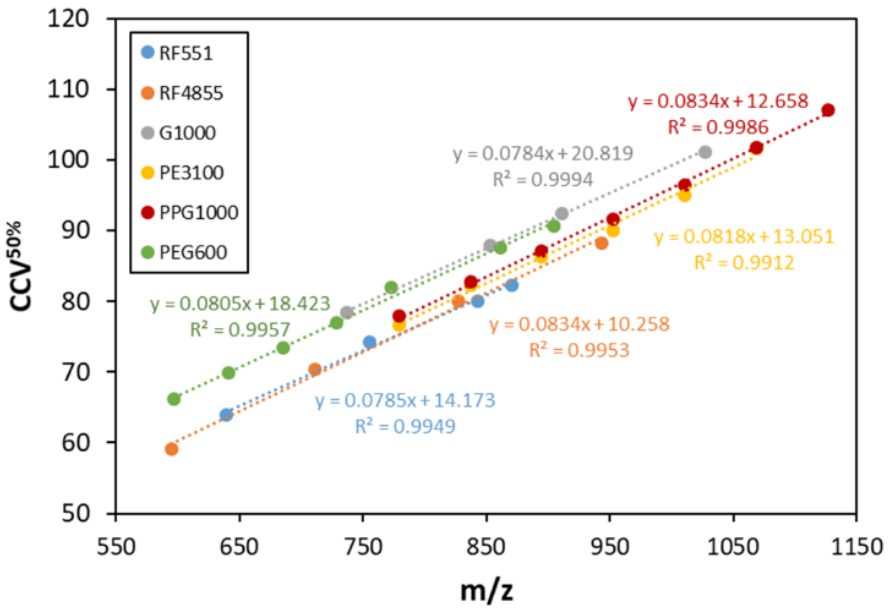

Figure 61 $CCV^{50\%}$ vs m/z plots of the polyether polyols.

Moreover, the intensities of the product ions were very small, and they were not suitable to select fragment peaks and to evaluate them. In this case, the differentiation of these compounds was not possible. That is the reason why $CCV^{20\%}$ was chosen and studied. This collision energy is optimal for all precursor ions of six different polyether polyols to fully characterize them.

5 SUMMARY

This dissertation presented the applications of data mining method – Mass-Remainder Analysis (MARA) for different complex systems. MARA is a method that processes a number of peaks and simplifies graphical representation of the (tandem) mass spectra. During this work the applicability of soft ionization mass spectrometry, including MALDI and ESI, for the epoxidized vegetable triglyceride oils, polymer blends and various types of polyether polyols was investigated.

First, MARA was used to characterize of the epoxidized vegetable oils, which are important polymer raw materials. Different epoxidized triglyceride series, such as triglycerides with 100% DOE (with all the double bonds converted to epoxide groups), triglycerides with one remaining double bond, or with diol side products were investigated. Number average molecular weight M_n, the average number (n_n^{NEG}) and average number of epoxide groups weighted by number of epoxide groups (n_w^{NEG}), the polydispersity of the number of epoxide groups (n_n^{NEG}/n_w^{NEG}), average number of carbon atoms (n_n^{C}), and the degree of epoxidation (DOE) of epoxidized soybean and linseed were determined. Furthermore, tandem mass spectrometric measurements were performed to explore the structural information of the epoxidized vegetable oils. It was found that sodium ETG adduct ions have very clear fragmentation pathways, in contrast to those of the other adducts (H^+, Li^+, and NH_4^+). Determining the epoxidized fatty acid composition of epoxidized triglyceride oils without any complicated and time-consuming sample preparation, derivatization, or separation is another advantage of MS/MS application. It can be applied to characterize the fatty acid variety of complex vegetable oil mixtures.

Second, MARA was developed to multi-step mass remainder analysis and used to differentiate between samples consisting of a single copolymer or

blend of copolymers. Different scenarios were performed, and appropriate base units was selected to plot simplified MARA graphs. For example, two copolymers with different repeat units in blends (PLA/PCL and PE3100) and two copolymers with the same repeat units in blends of (RF551-PE3100) and (RPE1740-PE8100). These copolymers with higher molecular weights showed complex mass spectra that completely hinder the presence of a blending component. M-MARA calculates sequentially mass-remainders and produces the graphical representation of the mass spectra of different copolymers, where the blending components can be identified. Applying MR_3 *versus* m/z plot, we easily recognized the presence of an additional series in polymer blend if the repeat units of those copolymers are different. If the repeat units of two copolymers are the same, the intensity scaled MR_2 *versus* MR_1 plots are suitable to differentiate the blend system based on their intensity distribution of the number of EO units. Therefore, M-MARA can be applied in quality control in polymer manufacturing industry. Moreover, applying the M-MARA method, multiple homologous series can be eliminated, presenting the similarities or differences in the chemical compositions.

Lastly, M-MARA was applied on the complex and peak-rich tandem spectra of various polyether polyols. The sequential calculation of the mass remainders easily eliminates the homologue series present in the mass spectra and produces the line with dots based on DBE values. For example, the maximum DBE value of 1, 2 and 4 indicates diol, glycerol- and sorbitol-based polyether polyols, respectively. The relationship between $CCV^{20\%}$ and the m/z values was found. It suggests an easy method to adjust the collision energy to get structural information, specifically to compare the polyether polyols based on the DBE values in M-MARA plots.

6 REFERENCES

[1] Painter, Paul C. and Coleman, Michael M. Fundamentals of polymer science: an introductory text. Lancaster, Pa.: Technomic Publication Co. (**1997**), 1

[2] Jenkins, A. D., Kratochvíl, P., Stepto, R. F. T., & Suter, U. W. Glossary of basic terms in polymer science (IUPAC Recommendations 1996). Pure and Applied Chemistry. (**1996**), 68(12), 2287–2311

[3] De, Sadhan K. Rubber Technologist's Handbook, Volume 1 (1st ed.). Smithers Rapra Press. (**1996**), 287

[4] Feldman, Dorel, and Alla Barbalata. Synthetic polymers: technology, properties, applications. Springer Science & Business Media (**1996**)

[5] S.J. Christian, Natural fibre-reinforced noncementitious composites (biocomposites), Nonconventional and Vernacular Construction Materials, Woodhead Publishing. (**2016)**, 111-126

[6] Wallace H. Carothers, Studies on polymerization and ring formation. An introduction to the general theory of condensation polymers, Journal of the American Chemical Society. (**1929**), 51 (8), 2548-2559

[7] Paul J Flory, Principles of Polymer Chemistry, Cornell University Press, Ithaca, NY, (**1953**)

[8] Odian, George. Principles of polymerization (4. ed.). Hoboken, NJ: Wiley-Interscience. (**2004**)

[9] Halasa, A. F. "Recent Advances in Anionic Polymerization". Rubber Chemistry and Technology. (**1981**), 54 (3): 627–640

[10] Cowie, J.M.G. Polymers chemistry and physics of modern materials (3rd ed / J.M.G. Cowie and Valeria Arrighi ed.). Boca Raton: Taylor & Francis (**2007**)

[11] Khalifeh, S. Introduction to polymers for electronic engineers. Polymers in Organic Electronics. (**2020**), 1–31

[12] Baeurle SA, Hotta A, Gusev AA. "On the glassy state of multiphase and pure polymer materials". Polymer. (**2006**), 47 (17): 6243–6253

[13] Horie, K., Barón, Máximo, Fox, R. B., He, J., Hess, M., Kahovec, J., Kitayama, T., Kubisa, P., Maréchal, E., Mormann, W., Stepto, R. F. T., Tabak, D., Vohlídal, J., Wilks, E. S. and Work, W. J. "Definitions of terms relating to reactions of polymers and to functional polymeric materials (IUPAC Recommendations 2003): " Pure and Applied Chemistry. (**2004**), 76(4), 889-906

[14] Penczek, S., Pretula, J., & Slomkowski, S. Ring-opening polymerization. Chemistry Teacher International. (**2021**), 3(2), 33–57

[15] Hargreaves, A. E.; Hargreaves, T. Chemical Formulation: An Overview of Surfactant-Based Preparations Used in Everyday Life; Royal Society of Chemistry: London. (**2003**); Vol. 32

[16] Dingels, C.; Schömer, M.; Frey, H. Die vielen Gesichter des Poly(ethylenglykol)s Chem. Unserer Zeit. (**2011**), 45, 338– 349

[17] Adam, Norbert; et al. "Polyurethanes". Ullmann's Encyclopedia of Industrial Chemistry. Weinheim: Wiley-VCH

[18] Ionescu, M. Chemistry and Technology of Polyols for Polyurethanes; Rapra Technology Limited: Shawbury, UK. (**2005**)

[19] O. Bayer, Das di-isocyanat-polyadditionsverfahren(polyurethane), Angewandte Chemie International Edition. (**1947)**, 59(9), 257–272

[20] Engels HW, Pirkl HG, Albers R, Albach RW, Krause J, Hoffmann A, Casselmann H, Dormish J. Polyurethanes: Versatile materials and sustainable problem solvers for today's challenges. Angewandte Chemie International Edition. (**2013**), 52:9422–41

[21] L. Mkrtchyan, M. Maier & U. Huber. Structural polyurethane foam: testing and modelling for automotive applications, International Journal of Crashworthiness. (**2008**), 13:5, 523-532

[22] Yasmina Boutar, Sami Naïmi, Salah Mezlini, Lucas F.M. da Silva, Moez Ben Sik Ali, Characterization of aluminium one-component polyurethane adhesive joints as a function of bond thickness for the automotive industry: Fracture analysis and behavior, Engineering Fracture Mechanics. (**2017**), 177, 45-60

[23] McKeen, L. W. Introduction to Plastics and Elastomers. The Effect of Creep and Other Time Related Factors on Plastics and Elastomers. (**2009**) 1–31

[24] BASF - Product information the chemicals catalog - Pluronics". BASF Corporation Website. (**2008**), 12-09

[25] Németh, Z., Rácz, G., & Koczo, K. Antifoaming action of polyoxyethylene-polyoxypropylene-polyoxyethylene-type triblock copolymers on BSA foams. Colloids and Surfaces A: Physicochemical and Engineering Aspects. (**1997**), 127(1-3), 151–162

[26] BASF Corporation, Brochure on Pluronic and Tetronic Surfactants. (**1989**), 6-8

[27] Terrier, P., Buchmann, W., Cheguillaume, G., Desmazières, B., & Tortajada, J. Analysis of Poly(oxyethylene) and Poly(oxypropylene) Triblock Copolymers by MALDI-TOF Mass Spectrometry. Analytical Chemistry. (**2005**), 77(10), 3292–3300

[28] Kabanov, A. V.; Lemieux, P.; Vinogradov, S.; Alakhov, V. Advanced Drug Delivery Reviews. (**2002)**, 54, 223-233

[29] Kabanov, A. V.; Batrakova, E. V.; Alakhov, V. J. Controlled Release. (**2002**), 82, 189-212

[30] BASF Corporation, Brochure on Technical Information of Pluronic® PE types, TI/ES 1026 e March **2005**

[31] BASF Corporation, Brochure on Technical Information of Pluronic® RPE types, TI/ES 1164 e April **2005**

[32] Ulery, B. D.; Nair, L. S.; Laurencin, C. T. Biomedical Applications of Biodegradable Polymers. Journal of Polymer Science Part B: Polymer Physics. (**2011**), 49 (12), 832-864

[33] PCC ROKITA, Brochure on Technical Information of ROKOPOL RF551

[34] Alakhova, D. Y., & Kabanov, A. V. Pluronics and MDR Reversal: An Update. Molecular Pharmaceutics. (**2014**), 11(8), 2566–2578.

[35] Alakhov, V.; Moskaleva, E.; Batrakova, E. V.; Kabanov, A. V. Hypersensitization of multidrug resistant human ovarian carcinoma cells by Pluronic P85 block copolymer. Bioconjugate Chemistry. (**1996**), 7, 209−216

[36] Batrakova, E. V.; Kabanov, A. V. Pluronic block copolymers: evolution of drug delivery concept from inert nanocarriers to biological response modifiers. Journal of Controlled Release. (**2008**), 130, 98−106

[37] Alakhova, D. Y.; Zhao, Y.; Li, S.; Kabanov, A. V. Effect of doxorubicin/Pluronic SP1049C on tumorigenicity, aggressiveness, DNA methylation and stem cell markers in murine leukemia. PLoS One. (**2013**), 8(8), e72238

[38] Parameswaranpillai, J., Thomas, S., & Grohens, Y. Polymer Blends: State of the Art, New Challenges, and Opportunities. Characterization of Polymer Blends. (**2014**), 1–6

[39] Paul, D.R. Control of phase structure in polymer blends, in Functional Polymers (eds D.E. Bergbreiter and C.R. Martin), Plenum Press, New York. (**1989**), 1–18

[40] Bermudez, J. M.; Grau, R. Thermosensitive poloxamer-based injectables as controlled drug release platforms for veterinary use: Development and in-vitro evaluation. International Research Journal of Pharmacy. (**2011**), 1 (6), 109-118

[41] Zhang, Y.; Tang, L.; Sun, L.; Bao, J.; Song, C.; Huang, L.; Liu, K.; Tian, Y.; Tian, G.; Li, Z.; Sun, H.; Mei, L. A novel paclitaxel-loaded poly(ε-caprolactone)/Poloxamer 188 blend nanoparticle overcoming multidrug resistance for cancer treatment. Acta Biomaterialia. (**2010**), 6 (6), 2045-2052

[42] Gupta, P. N.; Jain, S.; Nehate, C.; Alam, N.; Khare, V.; Dubey, R. D.; Saneja, A.; Kour, S.; Singh, S. K. Development and evaluation of paclitaxel loaded PLGA:poloxamer blend nanoparticles for cancer chemotherapy. International Journal of Biological Macromolecules. (**2014**), 69, 393-399

[43] Begum, S. A., Rane, A. V., & Kanny, K. Applications of compatibilized polymer blends in automobile industry. Compatibilization of Polymer Blends. (**2020**), 563–593

[44] Chung PC, Green PF. The elastic mechanical response of nanoscale thin films of miscible polymer/polymer blends. Macromolecules. (**2015**), 48(12), 3991-3996

[45] Santra RN, Mukundo PG, Chaki TK, Nando GB. Thermogravimetric studies on miscible blends of ethyleneemethyl acrylate copolymer (EMA) and poly dimethyl siloxane rubber (PDMS). Thermochimica Acta. (**1993**), 219:283-92

[46] Lizymol PP, Thomas S. Thermal behavior of polymer blends: a comparison of the thermal properties of miscible and immiscible systems. Polymer Degradation and Stability. (**1993**), 41:59-64

[47] Ameen S, Ali V, Zulfequar M, Mazharul Haq M, Husain M. Synthesis and characterization of polyaniline-polyvinyl chloride blends doped with sulfamic acid in aqueous tetrahydrofuran. Open Chemistry. (**2006**), 4:565-77

[48] Takahashi S, Okada H, Nobukawa S, Yamaguchi M. Optical properties of polymer blends composed of poly(methyl methacrylate) and ethyleneevinyl acetate copolymer. European Polymer Journal. (**2012**), 48(5), 974-980

[49] Robeson, L. M. Applications of polymer blends: Emphasis on recent advances. Polymer Engineering and Science. (**1984**), 24(8), 587–597

[50] Holser, Ronald A. "Transesterification of epoxidized soybean oil to prepare epoxy methyl esters". Industrial Crops and Products. (**2008**), 27: 130–132

[51] Liu, Z.; Erhan, S.Z. Ring-opening polymerization of epoxidized soybean oil. Journal of the American Oil Chemists' Society. (**2010**), 87, 437–444

[52] Grishchuk, S.; Karger-Kocsis, J. Hybrid thermosets from vinyl ester resin and acrylated epoxidized soybean oil (aeso). EXPRESS Polymer Letters. (**2011**), 5, 2–11

[53] H. Schuster, L. A. Rios, P. P. Weckes and W. F. Hoelderich, Applied Catalysis A. (**2008**), 348, 266 —270

[54] J. O. Metzger, European Journal of Lipid Science and Technology. (**2009**), 111, 865 —876

[55] Fernandez, A. M.; Murphy, C. J.; DeCosta, M. T.; et al. In Polymer Applications of Renewable-Resource Materials, Carraher C. E.; Sperling, L. H., Eds.; Plenum Press, New York. (**1983**)

[56] Rosch, J.; Mulhaupt, R. Polymer Bull. (**1993**), 31,679

[57] Hodakowski, L. E.; Osborn, C. L.; Harris, E. B. U.S. Patent 4,119,640; (**1975**)

[58] Likavec, W. R.; Bradley, C. R. U.S. Patent 5,866,628; (**1999**)

[59] Trecker, D. J.; Borden, G. W.; Smith, O. W. U.S. Patent 3,979,270; (**1976**)

[60] Bordon, G. W.; Smith, O. W.; Trecker, D. J. U.S. Patent 4,025,477; (**1974**)

[61] Blayo, A.; Gandini, A.; Le Nest, J.-F. Chemical and rheological characterizations of some vegetable oils derivatives commonly used in printing inks. Industrial Crops and Products. (**2001**), 14, 155–167

[62] Chai, C.; Ju, H.K.; Kim, S.C.; Park, J.H.; Lim, J.; Kwon, S.W.; Lee, J. Determination of bioactive compounds in fermented soybean products using

gc/ms and further investigation of correlation of their bioactivities. Journal of Chromatography B. (**2012**), 880, 42–49

[63] Murad, A.M.; Vianna, G.R.; Machado, A.M.; da Cunha, N.B.; Coelho, C.M.; Lacerda, V.A.M.; Coelho, M.C.; Rech, E.L. Mass spectrometry characterisation of fatty acids from metabolically engineered soybean seeds. Analytical and Bioanalytical Chemistry. (**2014**), 406, 2873–2883

[64] Thomson, J. J. Bakerian lecture: — rays of positive electricity. Proceedings of the Royal Society A. (**1913**), 89, 1–20

[65] Aston F.W., The Mass-Spectra of Chemical Elements, Phil. Mag. (**1919**), XXXXVIII, 707

[66] Bennett C.L., Beukens R.P., Clover M.R., Gove H.E., Liebert R.B., Litherland A.E., Purser K.H., Sondheim W.E., Radiocarbon Dating Using Electrostatic Accelerators: Negative Ions Provide the Key, Science. (**1977**), 198, 4316, 508

[67] Stephens W., Pulsed Mass Spectrometer with Time Dispersion, Bull. American Physical Society. (**1946**), 21, 2, 22

[68] Hipple J.A., Sommer H., Thomas H.A., A Precise Method of Determining the Faraday by Magnetic Resonance, Physical Review. (**1949**), 76, 12, 1877

[69] Paul W., Steinwedel H., Ein neues Massenspektrometer ohne Magnetfeld, Z. Naturforschg. (**1953**), 8a, 448

[70] Comisarow M.B., Marshall A.G., Fourier transform ion cyclotron resonance [FT-ICR] spectroscopy, Chemical Physics Letters. (**1974**), 25, 2, 282

[71] Makarov A., Electrostatic Axially Harmonic Orbital Trapping: A High-Performance Technique of Mass Analysis, Analytical Chemistry. (**2000**), 72, 6, 1156

[72] Dole M., Mack L.L., Hines R.L., Mobley R.C., Ferguson L.D., Alice M.B., Molecular beams of macroions, Journal of Chemical Physics. (**1968**), 49, 5, 2240

[73] Carroll D.I., Dzidic I., Stillwell R.N., Haegele K.D., Horning E.C., Atmospheric Pressure Ionization Mass Spectrometry: Corona Discharge Ion Source for Use in Liquid Chromatograph - Mass Spectrometer - Computer Analytical System, Analytical Chemistry. (**1975**), 47, 14, 2369

[74] Tanaka K., Waki H., Ido Y., Akita S., Yoshida Y., Yoshida T., Protein and polymer analysis up to m/z 100,000 by laser ionization time-of-flight mass spectrometry, Rapid Commun. Mass Spectrom. (**1988**), 2, 8, 151

[75] Bernhard Wolf. Handbook of Ion Sources. CRC Press. (**1995**)

[76] Ian G. Brown. The Physics and Technology of Ion Sources. John Wiley & Sons. (**2006**)

[77] Hillenkamp, Franz; Karas, Michael; Beavis, Ronald C.; Chait, Brian T. "Matrix-assisted laser desorption/ionization mass spectrometry of biopolymers". Analytical Chemistry. (**1991**), 63 (24): 1193A–1203A

[78] Ho, CS; Chan MHM; Cheung RCK; Law LK; Lit LCW; Ng KF; Suen MWM; Tai HL. "Electrospray Ionisation Mass Spectrometry: Principles and Clinical Applications". Clinical Biochemist Reviews. (**2003**), 24 (1): 3–12

[79] Covey, T. R., Thomson, B. A., & Schneider, B. B. Atmospheric pressure ion sources. Mass Spectrometry Reviews. (**2009**), 28(6), 870–897

[80] Karas, M., Bachmann, D., Bahr, U. and Hillenkamp, F. International Journal of Mass Spectrometry and Ion Processes. (**1987**), 78, 53

[81] Karas, M. and Hillenkamp, F.H. Analytical Chemistry. (**1988**), 60, 2229

[82] The Nobel Prize in Chemistry 2002. NobelPrize.org. Nobel Prize https://www.nobelprize.org/prizes/chemistry/2002/summary

[83] Stump, M.J., Fleming, R.C., Gong, W.-H. et al. Applied Spectroscopy. Rev. (**2002**), 37, 275

[84] Chapman, J. R. Methods in Mol. Biol.; Humana Press: Totowa, NJ. (**1996**), Vol. 61

[85] Dreisewerd, K. Chemical Reviews. (**2003**), 103, 395

[86] Mann, M., Meng, C.K. and Fenn, J.B. Interpreting mass spectra of multiply charged ions. Analytical Chemistry. (**1989**), 61, 1702–8

[87] de la Mora, J.F., Van Berkel, G.J., Enke, C.G. et al. Electrochemical processes in electrospray ionization mass spectrometry. Journal of Mass Spectrometry. (**2000**), 35, 939–52

[88] Cech, N.B. and Enke, C.G. Practical implications of some recent studies in electrospray ionization fundamentals. Mass Spectrometry Reviews. (**2001**), 20, 362–87

[89] Rohner, T.C., Lion, N. and Girault, H.H. Electrochemical and theoretical aspects of electrospray ionisation. Physical Chemistry Chemical Physics. (**2004**), 6, 3056–68

[90] Banerjee, S., & Mazumdar, S. Electrospray Ionization Mass Spectrometry: A Technique to Access the Information beyond the Molecular

Weight of the Analyte. International Journal of Analytical Chemistry. (**2012**), 1–40

[91] Marginean, I., Kelly, R. T., Prior, D. C., LaMarche, B. L., Tang, K., & Smith, R. D. Analytical Characterization of the Electrospray Ion Source in the Nanoflow Regime. Analytical Chemistry. (**2008**), 80(17), 6573–6579

[92] Shen, Y., Tolić, N., Zhao, R., Paša-Tolić, L., Li, L., Berger, S. J., Smith, R. D. High-Throughput Proteomics Using High-Efficiency Multiple-Capillary Liquid Chromatography with On-Line High-Performance ESI FTICR Mass Spectrometry. Analytical Chemistry. (**2001**), 73(13), 3011–3021

[93] Krenkova, J., & Foret, F. On-line CE/ESI/MS interfacing: Recent developments and applications in proteomics. PROTEOMICS. (**2012**), 12(19-20), 2978–2990

[94] Tubaon, R. M., Haddad, P. R., & Quirino, J. P. Sample Clean-up Strategies for ESI Mass Spectrometry Applications in Bottom-up Proteomics: Trends from 2012 to 2016. PROTEOMICS. (**2017**), 17(20), 1700011

[95] Edmond de Hoffmann, Vincent Stroobant, Mass Spectrometry: Principles and Applications, 3rd Edition, 2007, Wiley

[96] Ferguson, R.E., McKulloh, K.E. and Rosenstock H.M. The Journal of Chemical Physics. (**1965**), 42, 100

[97] Kienitz, H. Massenspektrometrie, Verlag Chemie, Weinheim. (**1968**)

[98] Mass spectrometers for vacuum, gas, plasma and surface science, Hiden Analytical Ltd

[99] Stephens, W. Physical Review. (**1946**), 69, 691

[100] Cotter, R.J. Analytical Chemistry. (**1999**), 71, 445A

[101] Guilhaus, M. Journal of Mass Spectrometry. (**1995**), 30, 1519

[102] Mann, M. and Talbo, G. Developments in matrix-assisted laser desorption/ ionization peptide mass spectrometry. Current Opinion in Biotechnology. (**1996**), 7, 11–9

[103] Mamyrin, B.A. Int. Journal of Mass Spectrometry. (**2001**), 206, 251–66

[104] Weickhardt, C., Moritz, F. and Grotemeyer, J. Time-of-flight mass spectrometry: state-of-the-art in chemical analysis and molecular science. Mass Spectrometry Reviews. (**1996**), 15(3), 139–62

[105] Greco, V., Piras, C., Pieroni, L., Ronci, M., Putignani, L., Roncada, P., & Urbani, A. Applications of MALDI-TOF mass spectrometry in clinical proteomics. Expert Review of Proteomics. (**2018**), 1–14

[106] Wiley, W. C.; McLaren, I. H. "Time-of-Flight Mass Spectrometer with Improved Resolution", Review of Scientific Instruments. (**1955**), 26 (12): 1150

[107] Mamyrin, B.A., Karataev, V.I., Schmikk, D.V. and Zagulin, V.A. Journal of Experimental and Theoretical Physics. (**1973**), 37, 4

[108] Kore Technology, Kore Components: TOF-MS Optics R-500 reflectron

[109] Brown, K. L.; G. W. Tautfest "Faraday-Cup Monitors for High-Energy Electron Beams" Review of Scientific Instruments. (**1956**), 27 (9): 696–702

[110] J. Rajchman and E.W. Pike, RCA Technical Report TR-362, "Electrostatic Focusing in Secondary Emission Multipliers." (**1937**)

[111] Donohue, D.L., Carter, J.A., & Mamantov, G. An electro-optical ion detector for spark source mass spectrometry. International Journal of Mass Spectrometry and Ion Physics. (**1980**), 33(1), 45-55

[112] Guilhaus, M. Mass spectrometry | Time-of-Flight. Encyclopedia of Analytical Science. (**2005**), 412–423

[113] Wiza, J. "Microchannel plate detectors". Nuclear Instruments and Methods. (**1979**), 162 (1–3): 587–601

[114] Allen, James S. "An Improved Electron Multiplier Particle Counter", Review of Scientific Instruments. (**1947**), 18 (10): 739–749

[115] Tao, S., Chan, H., & van der Graaf, H. Secondary Electron Emission Materials for Transmission Dynodes in Novel Photomultipliers: A Review. (**2016**), Materials, 9 (12), 1017

[116] Glish, G. L., & Vachet, R. W. The basics of mass spectrometry in the twenty-first century. Nature Reviews Drug Discovery. (**2003**), 2(2), 140–150

[117] De Hoffmann, E. Tandem mass spectrometry: A primer. Journal of Mass Spectrometry. (**1996**), 31(2), 129–137

[118] Armentrout, P.B. Threshold collision-induced dissociations for the determination of accurate gas-phase binding energies and reaction barriers. Topics in current chemistry. (**2003**), 225. 233-262

[119] Muntean, F., & Armentrout, P. B. Guided ion beam study of collision-induced dissociation dynamics: integral and differential cross sections. The Journal of Chemical Physics. (**2001**), 115(3), 1213–1228

[120] K. Levsen, Fundamental Aspects of Organic Mass Spectrometry, Verlag Chemie: Weinheim, New York. (**1978**), 138

[121] Gabelica, V., & Pauw, E. D. Internal energy and fragmentation of ions produced in electrospray sources. Mass Spectrometry Reviews. (**2005**), 24(4), 566–587

[122] Sleno, L., & Volmer, D. A. Ion activation methods for tandem mass spectrometry. Journal of Mass Spectrometry. (**2004**), 39(10), 1091–1112

[123] Louris JN, Wright LG, Cooks RG, Schoen AE. "New scan modes accessed with a hybrid mass spectrometer". Analytical Chemistry. (**1985**), 57 (14): 2918–2924

[124] Lin, S.-Y., Hsu, W.-H., Lin, C.-C., & Chen, C.-J. Mass spectrometry-based proteomics in Chest Medicine, Gerontology, and Nephrology: subgroups omics for personalized medicine. (**2014**)

[125] Imbert, Y., Arnaud, R., Tabet, J.C. and de Hoffmann, E. Gas phase reaction of neutral carbon disulfide with its hydride adduct anion: tandem mass spectrometry and theoretical studies. The Journal of Physical Chemistry. (**1998**), 102, 3732–7

[126] Cooks, R.G., Patrick, J.S., Kotiaho, T. and McLuckey, S.A. Mass Spectrometry Reviews. (**1994**), 13, 287

[127] Cooks, R.G. and Wong, P.S.H. Accounts of Chemical Research. (**1998**), 31, 379

[128] Nagy, T., Kuki, Á., Zsuga, M., & Kéki, S. Mass-Remainder Analysis (MARA): a New Data Mining Tool for Copolymer Characterization. Analytical Chemistry. (**2018**), 90(6), 3892–3897

[129] Nagy, T., Kuki, Á., Nagy, M., Zsuga, M., & Kéki, S. Mass-Remainder Analysis (MARA): An Improved Method for Elemental Composition

Assignment in Petroleomics. Analytical Chemistry. (**2019**), 21;91(10), 6479-6486.

[130] Kendrick, E. Analytical Chemistry. (**1963**), 35, 2146−2154

[131] Van Krevelen, D. Fuel. (**1950**), 29, 269−284

[132] Fouquet, T.; Sato, H. Analytical Chemistry. (**2017**), 89, 2682−2686

LIST OF PUBLICATIONS

Publications related to the dissertation:

1. **Title:** Mass Spectrometric Characterization of Epoxidized Vegetable Oils
   Authors: Ákos Kuki, Tibor Nagy, **Mahir Hashimov**, Stella File, Miklós Nagy, Miklós Zsuga and Sándor Kéki
   Journal Details: Polymers 2019, 11(3), 394 [**IF**: 4.33] https://doi.org/10.3390/polym11030394

2. **Title:** Multistep Mass-Remainder Analysis and its Application in Copolymer Blends
   Authors: Tibor Nagy, Ákos Kuki, **Mahir Hashimov**, Miklós Zsuga, and Sándor Kéki
   Journal Details: Macromolecules 2020, 53, 4, 1199–1204, [**IF**: 5.91] https://doi.org/10.1021/acs.macromol.9b02409

3. **Title:** Tandem Mass-Remainder Analysis of Industrially Important Polyether Polyols
   Authors: Mahir Hashimov, Ákos Kuki, Tibor Nagy, Miklós Zsuga, and Sándor Kéki
   Journal Details: Polymers 2020, 12(12), 2768; [**IF**: 4.33] https://doi.org/10.3390/polym12122768

Other publications:

4. **Title:** Polydispersity Ratio and Its Application for the Characterization of Poloxamers

   Authors: Gergő Róth, Tibor Nagy, Ákos Kuki Ákos Kuki, **Mahir Hashimov**, Zsófia Vonza, István Timári, Miklós Zsuga, and Sándor Kéki

   Journal Details: Macromolecules 2021, 54, 21, 9984–9991 [**IF**: 5.91] https://doi.org/10.1021/acs.macromol.1c01552

CONFERENCES

Conferences related to the dissertation:

1. **Hashimov, M**.; Nagy, T.; Kuki, Á.; Zsuga, M.; Kéki, S. Tandem Mass Spectrometric Characterization of Sorbitol-Initiated Polyethers. XXV. International Conference on Chemistry 2019, Cluj-Napoca, Romania.

2. File, S.; Kuki, Á.; Nagy, T.; **Hashimov, M**.; Nagy, M.; Zsuga, M.; Kéki, S. Characterization of epoxidized soybean and linseed oil by mass spectrometry. XXV. International Conference on Chemistry 2019, Cluj-Napoca, Romania.

3. Kuki, Á.; Nagy, T.; **Hashimov, M**.; File, S.; Nagy, M.; Zsuga, M.; Kéki, S. Determination of the fatty acid compositions of epoxidized vegetable oils by tandem mass spectrometry. XXV. International Conference on Chemistry 2019, Cluj-Napoca, Romania.

4. Nagy, T.; Kuki, Á.; **Hashimov, M**.; Zsuga, M.; Kéki, S. Mass-remainder Analysis (MARA): a multifunctional tool for characterization of copolymers and copolymer blends. ESOPS 2020, Linz, Austria.

5. Nagy, T.; Kuki, Á.; **Hashimov, M**.; Zsuga, M.; Kéki, S.; Characterization of copolymer blends by Mass-Remainder Analysis. XXVI. International Conference on Chemistry 2020, Cluj-Napoca, Romania.

6. **Hashimov, M**.; Kuki, Á.; Nagy, T.; Zsuga, M.; Kéki, S.; Application of Multistep Mass-Remainder Analysis for the evaluation copolymer tandem mass spectra. XXVI. International Conference on Chemistry 2020, Cluj-Napoca, Romania.

7. **Hashimov, M**.; Kuki, Á.; Nagy, T.; Zsuga, M.; Kéki, S.; Importance of Mass-Remainder Analysis (MARA) in Polymer Characterization. Young Researchers' International Conference on Chemistry and Chemical Engineering (YRICCCE III) 2021, Cluj-Napoca, Romania.

Other conferences:

8. **Hashimov, M.**; Nagy, T.; Kuki, Á.; Zsuga, M.; Kéki, S. Rapid determination of PEG 400 excreted in the urine. XXVII. International Conference on Chemistry 2021, Cluj-Napoca, Romania.

9. Nagy, T.; Roth, G.; Kuki, Á.; **Hashimov, M.**; Timari, I.; Vonza, Zs.; Zsuga, M.; Kéki, S. Application of polydispersity ratio on the analysis of copolymers. XXVII. International Conference on Chemistry 2021, Cluj-Napoca, Romania.

10. **Hashimov, M.**; Nagy, T.; Kuki, Á.; Zsuga, M.; Kéki, S. Determination of polyethylene glycol 400 excreted in the urine by MALDI coupled to time-of-flight mass spectrometry. 10th Interdisciplinary Doctoral Conference (IDK2021) 2021, Pécs, Hungary.

Posters related to the dissertation:

1. **Hashimov, M.**; Nagy, T.; Kuki, Á.; Zsuga, M.; Kéki, S. Characterization of various polyether polyols by Mass Spectrometry. ESOPS 2020, Linz, Austria.

2. Kuki, Á.; Nagy, T.; **Hashimov, M**.; File, S.; Nagy, M.; Zsuga, M.; Kéki, S. Mass spectrometric characterization of epoxidized vegetable oils for biopolymers. ESOPS 2020, Linz, Austria.

3. **Hashimov, M.**; Kuki, Á.; Nagy, T.; Zsuga, M.; Kéki, S. Mass spectrometric characterization of epoxidized vegetable oils. 1st UFAZ-ASOIU-UNISTRA scientific conference 2021, Baku, Azerbaijan.

Other posters:

4. **Hashimov, M**.; Kuki, Á.; Nagy, T.; Zsuga, M.; Kéki, S.; Rapid detection of fire-retardant compounds by direct analysis in real-time mass spectrometry, European Meeting on Fire Retardant Polymeric Materials (FRPM21) 2021, Budapest, Hungary

AWARDS

1. Young Researchers Fellowship 2019

Research topic: Study of reactivity and fragmentation of epoxidized triglycerides by mass spectrometry

Issue date: April 2019

Issuer: European Union and the European Social Fund, Debrecen Venture Catapult Program - Széchenyi 2020

2. Young Researchers Fellowship 2021

Research topic: Fractionation and characterization of epoxidized vegetable oils and a study of the evolution of physical properties of polymers formed by photopolymerizations of different epoxidized triglycerides

Issue date: January 2021

Issuer: European Union and the European Social Fund, Debrecen Venture Catapult Program - Széchenyi 2021